α-cluster structure and density waves in oblate nuclei

Yoshiko Kanada-En'yo
Department of Physics, Kyoto University, Kyoto 606-8502, Japan

Yoshimasa Hidaka
Mathematical Physics Laboratory, RIKEN Nishina Center, Saitama 351-0198, Japan

(Received 20 April 2011; published 14 July 2011)

Pentagon and triangle shapes in ^{28}Si and ^{12}C are discussed in relation to nuclear density waves. In the antisymmetrized molecular dynamics calculations, the $K^\pi = 5^-$ band in ^{28}Si and the $K^\pi = 3^-$ band in ^{12}C are described by the pentagon and triangle shapes, respectively. These negative-parity bands can be interpreted as the parity partners of the $K^\pi = 0^+$ ground bands and they are constructed from the parity-asymmetric-intrinsic states. The pentagon and the triangle shapes originate in 7α- and 3α-cluster structures, respectively. In a mean-field picture, they are described also by the static one-dimensional density waves at the edge of the oblate states. In analyses with ideal α-cluster models using Brink-Bloch cluster wave functions and that with a simplified model, we show that the static edge density waves for the pentagon and triangle shapes can be understood by spontaneous breaking of axial symmetry, i.e., the instability of the oblate states with respect to the edge density waves. The density wave is enhanced in the $Z = N$ nuclei due to the proton-neutron coherent density waves, while it is suppressed in $Z \neq N$ nuclei.

DOI: 10.1103/PhysRevC.84.014313 PACS number(s): 21.10.−k, 21.60.Gx

I. INTRODUCTION

In light nuclei, some negative-parity rotational bands with high K quanta are discussed in relation to specific symmetry of intrinsic states. One of the most famous examples is the 3^- state at 9.64 MeV in ^{12}C, which has been discussed for a long time in connection to an equilateral triangle configuration of 3α-cluster structure. The 3^- state is the lowest negative-parity state, and its spin contradicts the naive expectation from shell-model calculations. The reason for the low-lying 3^- state can be understood by the point group D_{3h} symmetry of the equilateral triangle 3α-cluster structure [1–3] [see Fig. 1(a)], which is characterized by the n-fold symmetry with $n = 3$ of the intrinsic structure. The 3^- state is interpreted as the bandhead of the $K^\pi = 3^-$ band constructed by the parity and total-angular-momentum projection from the D_{3h} symmetry of the intrinsic state. Although the 4^- state in the $K^\pi = 3^-$ band has not yet been confirmed, a possible assignment of 4^- for the level at 13.35 MeV was suggested [4]. In microscopic 3α-cluster models, the $K^\pi = 3^-$ band is considered to form a parity doublet with the $K^\pi = 0^+$ ground band [5].

In ^{28}Si, the $K^\pi = 5^-$ rotational band starting from the 5^-_1 state at 9.70 MeV was reported in γ-ray measurements by Glatz *et al.* [6], and it was discussed with a 7α-cluster structure with a pentagon shape [7,8]. In the 7α-cluster model with Brink-Bloch (BB) α-cluster wave functions [1], an oblate solution for negative parity shows the D_{5h} symmetry [see Fig. 1(b)]. Since a $K^\pi = 5^-$ band can be constructed from the D_{5h} symmetry of the intrinsic state, the existing $K^\pi = 5^-$ band might be indirect evidence of the pentagon shape and may be regarded as the parity partner of the $K^\pi = 0^+$ ground state.

In spite of the reasonable description of the $K^\pi = 5^-$ band in ^{28}Si with the 7α-cluster model, the BB α-cluster model is too simple to quantitatively describe the low-lying energy spectra of ^{28}Si [8]. Moreover, the validity of the ansatz that ^{28}Si consists of seven α clusters is not obvious but it should be checked within frameworks without any cluster assumptions because α clusters might be dissociated or melted down due to the spin-orbit force in sd-shell nuclei [9].

Recently, more sophisticated calculations of ^{28}Si were performed by one of the authors with antisymmetrized molecular dynamics (AMD) [10,11], which is a framework free from cluster assumptions. The calculations reproduce well low-lying positive-parity levels of the oblate ground band and the excited prolate band by incorporating the spin-orbit force with a proper strength. Interestingly, the $K^\pi = 5^-$ band is constructed from the oblate state with a pentagon shape even though existence of any clusters is not assumed in the calculations [11]. This means that the pentagon shape can be induced by α-cluster correlation in the oblate intrinsic state of ^{28}Si.

From the viewpoint of the symmetry breaking, the pentagon shape in the intrinsic state is regarded as the spontaneous breaking of axial symmetry. The surface density is oscillating along the edge of the oblate shape, that is, spontaneous symmetry breaking (SSB) occurs in the rotational invariance around the symmetric axis. In relation to SSB, this structure is associated with density waves (DWs) in nuclear matter, in which SSB of the translational invariance occurs. Density waves in nuclear matter have been discussed for a long time [12–14], and it was suggested that a one-dimensional DW could be stable in low-density nuclear matter [14]. Nonuniform nuclear matter with density oscillations has also been investigated with cluster models such as α-cluster matter [15–17]. In analogy to nuclear matter DWs, the pentagon shape can be interpreted as the static one-dimensional DW at the edge of the oblate state. Our aim is to give a description of the pentagon and triangle shapes in terms of DWs with

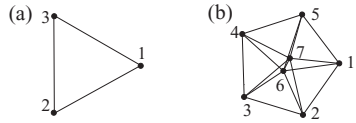

FIG. 1. The schematic figures for spatial configurations of cluster centers of (a) a triangle structure consisting of three α clusters in ^{12}C and (b) a pentagon structure of seven α clusters in ^{28}Si.

wave numbers five and three, respectively, to discuss the relation of the 7α- and 3α-cluster structures to the static edge DWs, i.e., spontaneous axial symmetry breaking of the oblate states.

In this paper, we report AMD calculations of ^{28}Si while focusing on the pentagon shape in the oblate states. By analyzing single-particle wave functions of the obtained AMD wave functions, we show that the pentagon shape is expressed by one-particle and one-hole excitations of an oblate state with a wave number five; this can be interpreted as a one-dimensional DW. To see the instability of axial symmetry with respect to the pentagon shape, analyses of ideal cluster models using BB wave functions are performed. Similarly, by focusing on the triangle shape of the 3α-cluster structure, structures of ^{12}C are also discussed. We introduce a simplified model for a one-dimensional DW in the oblate state by truncating active orbits for particle and hole states, and we show that the proton-neutron coherent DWs in $Z = N$ nuclei promote the instability of the oblate states with respect to the pentagon and triangle shapes. The suppression mechanism of cluster structures in neutron-rich nuclei is discussed from the viewpoint of proton DWs with excess neutrons.

The paper is organized as follows: In the next section, we explain the AMD calculations for ^{28}Si and ^{12}C. Analyses with ideal cluster models using BB α-cluster wave functions are given in Sec. III, and those using extended BB wave functions in Sec. IV. Discussions with a simplified model for the one-dimensional DW are given in Sec. V. Finally, in Sec. VI, a summary and an outlook are given.

II. AMD CALCULATIONS FOR ^{28}Si AND ^{12}C

A. Method of AMD calculations

The AMD method has been applied for various nuclei and has been successful in describing shell-model structures and cluster structures of ground and excited states in the light-mass region [18–20]. Here we briefly describe a simple version of the AMD method and its application to ^{28}Si and ^{12}C [10,18], focusing on cluster features of the oblate bands. The details of the previous AMD calculations for ^{28}Si are described in Refs. [10,11], in which the energy levels of the $K^\pi = 0^+_1$, $K^\pi = 0^+_2$, $K^\pi = 3^-$, and $K^\pi = 5^-$ bands are well reproduced.

An AMD wave function for an A-nucleon system is given by a Slater determinant of Gaussian wave packets,

$$\Phi_{\rm AMD}(\mathbf{Z}) = \frac{1}{\sqrt{A!}}\mathcal{A}\{\varphi_1, \varphi_2, \ldots, \varphi_A\}, \tag{1}$$

where the ith single-particle wave function is written as

$$\varphi_i = \phi_{\mathbf{Z}_i}\mathcal{X}_i, \tag{2}$$

$$\phi_{\mathbf{Z}_i}(\mathbf{r}_j) \propto \exp\left[-\nu\left(\mathbf{r}_j - \frac{\mathbf{Z}_i}{\sqrt{\nu}}\right)^2\right]. \tag{3}$$

Here $\mathcal{X}_i$ is the spin-isospin function and fixed to be $p\uparrow$, $p\downarrow$, $n\uparrow$, or $n\downarrow$. The spatial part is represented by complex variational parameters, Z_{xi}, Z_{yi}, Z_{zi}, which indicate the centers of the ith Gaussian wave packet. The parameter ν is chosen to be $\nu = 0.15$ fm^{-2} and $\nu = 0.175$ fm^{-2} for ^{28}Si and ^{12}C so as to minimize the energy of the positive-parity state.

In the AMD model, all the centers $\{\mathbf{Z}_1, \mathbf{Z}_2, \ldots, \mathbf{Z}_A\}$ of single-nucleon Gaussians are treated independently as complex variational parameters. Thus, the AMD method is based completely on single nucleons and therefore it is free from such assumptions as cluster existence or axial symmetry. Nevertheless, if a cluster structure is favored in a system, the cluster structure can be described as an optimum solution of AMD wave functions because BB cluster wave functions are included in the AMD model space. For instance, α-cluster formation is expressed by the concentration of Gaussian centers for four nucleons, $p\uparrow$, $p\downarrow$, $n\uparrow$, and $n\downarrow$, at a certain position.

By using an effective Hamiltonian,

$$H_{\rm eff} = \sum_i T_i + \sum_{i<j} v_{ij} + \sum_{i<j<k} v_{ijk}, \tag{4}$$

consisting of kinetic terms and two-body and three-body interaction terms as effective nuclear forces, the energy variation is performed within the AMD model space to obtain the optimum solutions, which correspond to the intrinsic wave functions for low-lying states. As in Refs. [10,11,18], the energy variation is done after parity projection by operating $(1 \pm P_r)$ on the AMD wave function. After obtaining the energy variation for $(1 \pm P_r)\Phi_{\rm AMD}(\mathbf{Z})$ with respect to $\mathbf{Z}$ the optimized intrinsic wave functions, $\Phi_{\rm AMD}(\mathbf{Z}^{(+)})$ and $\Phi_{\rm AMD}(\mathbf{Z}^{(-)})$, are obtained for the positive- and negative-parity states, respectively. Then, the total-angular-momentum projection, P^J_{MK}, is operated on the obtained AMD wave functions, $P^J_{MK}(1 \pm P_r)\Phi_{\rm AMD}$, to calculate expectation values of parity and angular-momentum eigenstates, $J^\pm$.

The adopted effective nuclear forces are the same as those in Refs. [10,11] with which AMD calculations reproduce the energy levels of ^{28}Si, namely, the MV1 force (case 1) [21], which consists of finite-range two-body and zero-range three-body forces, with a parameter set ($b = h = 0, m = 0.62$) used for the central force. As for the spin-orbit force, the spin-orbit term of the G3RS force [22] with strengths $u_I = -u_{II} =$ 2800 MeV is adopted. The Coulomb force is approximated by seven Gaussians.

Using these interactions, the binding energies of ^{28}Si and ^{12}C are calculated to be 207.5 and 80.6 MeV, respectively, with the AMD calculations. The calculations somehow underestimate the experimental binding energies, 236.53 and 92.16 MeV. For quantitative reproduction, fine tuning of interaction parameters is possible. However, the intrinsic

structures and energy levels are not so sensitive to such parameter tuning and the following results should be almost unchanged.

B. AMD results for ^{28}Si

In the present work, we focus only on the oblate rotational bands, $K^\pi = 0^+_1$, $K^\pi = 3^-_1$, and $K^\pi = 5^-_1$, though the prolate excited $K^\pi = 0^+_2$ band exists in ^{28}Si [10]. We adopt the oblate solutions of the intrinsic wave functions $\Phi_{\rm AMD}(\mathbf{Z}^{(+)})$ and $\Phi_{\rm AMD}(\mathbf{Z}^{(-)})$ obtained by energy variation after positive- and negative-parity projections. $\Phi_{\rm AMD}(\mathbf{Z}^{(+)})$ and $\Phi_{\rm AMD}(\mathbf{Z}^{(-)})$ correspond to the intrinsic states of the lowest positive- and negative-parity bands. The density distributions of these AMD wave functions are shown in Fig. 2. Interestingly, the wave function $\Phi_{\rm AMD}(\mathbf{Z}^{(+)})$, which corresponds to the $K^\pi = 0^+$ ground band, shows the pentagon shape due to the 7α-like structure even though α clusters are not *a priori* assumed in the framework. We should comment that α clusters in $\Phi_{\rm AMD}(\mathbf{Z}^{(+)})$ are somehow dissociated due to the spin-orbit force as discussed in Ref. [10]. From these two intrinsic states $\Phi_{\rm AMD}(\mathbf{Z}^{(+)})$ and $\Phi_{\rm AMD}(\mathbf{Z}^{(-)})$, we calculate the $J^\pm$ states by performing parity and angular-momentum projections and diagonalizing the Hamiltonian and norm matrices with respect to $P^J_{MK}(1 \pm P_r)\Phi_{\rm AMD}(\mathbf{Z}^{(+)})$ and $P^J_{MK}(1 \pm P_r)\Phi_{\rm AMD}(\mathbf{Z}^{(-)})$. Here, states with each parity are described by a linear combination of the parity and angular-momentum eigenstates projected from both $\Phi_{\rm AMD}(\mathbf{Z}^{(+)})$ and $\Phi_{\rm AMD}(\mathbf{Z}^{(-)})$. The calculated energy levels of ^{28}Si compared with the experimental data of the members in the oblate bands $K^\pi = 0^+_1$, $K^\pi = 3^-_1$, and $K^\pi = 5^-_1$ are shown in Fig. 3. The experimental energy levels are reproduced rather well by the calculations. The calculated in-band $E2$ transition strengths also reproduce well the experimental data (see Table. I). The ground band, $K^\pi = 0^+_1$, and the lowest negative-parity band, $K^\pi = 3^-_1$, are dominantly constructed from $\Phi_{\rm AMD}(\mathbf{Z}^{(+)})$ and $\Phi_{\rm AMD}(\mathbf{Z}^{(-)})$, respectively. The $K^\pi = 5^-_1$ band is mainly constructed from $\Phi_{\rm AMD}(\mathbf{Z}^{(+)})$ having the pentagon shape though the $K^\pi = 5^-_1$ band member states have significant mixing with the $K^\pi = 3^-_1$ band members. This means that the $K^\pi = 0^+_1$ and the $K^\pi = 5^-_1$ bands can be interpreted as parity partners constructed from the parity-asymmetric-intrinsic state $\Phi_{\rm AMD}(\mathbf{Z}^{(+)})$ with the pentagon shape.

Next we analyze the single-particle wave functions in the pentagon intrinsic state. The single-particle wave functions φ_i in Eq. (2) written in terms of Gaussian wave packets are nonorthogonal to each other. We can make a linear transformation from the set $\{\varphi_i\}$ to an orthonormal basis set $\{\varphi'_i\}$ by keeping the Slater determinant unchanged except for normalization, $\det\{\varphi'_i\} \propto \det\{\varphi_i\} = \Phi_{\rm AMD}(\mathbf{Z})$. From this orthonormal basis, we construct the Hartree-Fock (HF) single particles $\{\varphi^{\rm HF}_i\}$, which diagonalize the HF single-particle Hamiltonian as described in Ref. [23]. Analysis of $\{\varphi^{\rm HF}_i\}$ is helpful to discuss intrinsic states in a mean-field picture.

Among the HF single-particle wave functions in the intrinsic wave function, $\Phi_{\rm AMD}(\mathbf{Z}^{(+)})$, we find single-particle orbits with pentagon density distributions (see Fig. 4). The pentagon orbits show parity asymmetry, indicating mixing of

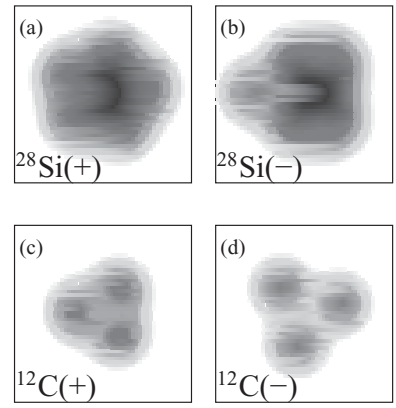

FIG. 2. Density distributions of the AMD wave functions for the positive- and negative-parity states in ^{28}Si and ^{12}C.

positive-parity and negative-parity components. We extract each parity component from the pentagon orbits, and we find that about a 5% negative-parity component is mixed in with the dominant positive-parity component in each orbit. As shown in Fig. 4, both the positive- and negative-parity components show donut shapes in their density distributions, and the pentagon orbits can be roughly described by a linear combination $c\phi_{(0,0,\pm2)} + c'\phi_{(0,0,\mp3)}$ with $|c'|^2 \sim 0.05$ for $|c|^2 + |c'|^2 = 1$, in terms of harmonic oscillator (H.O.) single-particle orbits labeled by quantum numbers (n_z, n_ρ, m_l) in cylinder coordinates. (See Appendix A for the expressions of $\phi_{(0,0,\pm2)}$ and $\phi_{(0,0,\pm3)}$.) In the pentagon state of ^{28}Si, a total of eight pentagon orbits are found, corresponding to $c\phi_{(0,0,\pm2)} + c'\phi_{(0,0,\mp3)}$ occupied by four species of nucleons, $p\uparrow$, $p\downarrow$, $n\uparrow$, and $n\downarrow$.

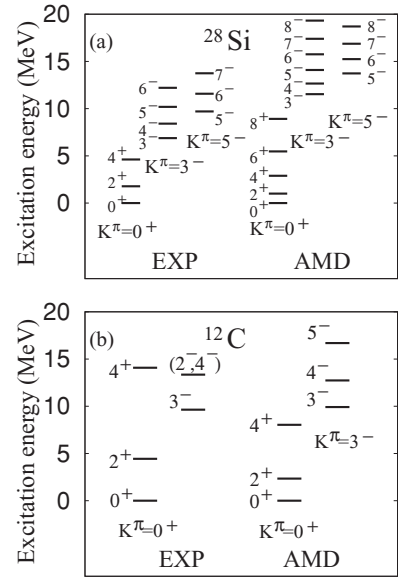

FIG. 3. (a) Energy levels calculated with AMD calculations and the experimental levels of the $K^\pi = 0^+_1$, $K^\pi = 3^-_1$, and $K^\pi = 5^-_1$ bands in ^{28}Si. (b) Energy levels of the $K^\pi = 0^+_1$ and $K^\pi = 3^-_1$ bands in ^{12}C. The experimental data are taken from Refs. [4,6].

TABLE I. The calculated and the experimental values of $E2$ transition strengths in ^{28}Si. The values in Weisskopf units, W.u. = 5.05 e^2fm^{-4} are listed. The $B(E2)$ values are calculated with the AMD method. The experimental data are taken from Ref. [6].

Initial $J_f^\pm$	Final $J_i^\pm$	$B(E2)$ exp.	$B(E2)$ calc.
$K^\pi = 0_1^+ \to 0_1^+$			
2_1^+	0_1^+	12.7(+0.4, −0.3)	10.6
4_1^+	2_1^+	13.6(+1.4, −1.2)	15.1
6_1^+	4_1^+	9.4(+3.6, −2.0)	16.2
$K^\pi = 3_1^- \to 3_1^-$			
4_1^-	3_1^-	32.4(+9.6, −6.4)	22.4
5_2^-	3_1^-	>3.4	2.0
5_2^-	4_1^-		13.7
6_2^-	4_1^-	>6.1	2.5
6_2^-	5_2^-	>12	16.9
7_2^-	5_2^-		5.2
7_2^-	6_2^-		16.9
8_2^-	6_2^-		7.8
$K^\pi = 5_1^- \to 5_1^-$			
6_1^-	5_1^-	17(+8, −4)	14.4
7_1^-	5_1^-	>2.5	7.7
7_1^-	6_1^-	>16.5	13.8
8_1^-	6_1^-		10.1
$K^\pi = 5_1^- \to 3_1^-$			
5_1^-	3_1^-	0.034(+0.01, −0.01)	4.0
5_1^-	4_1^-	2(+0.2, −0.2)	7.1
7_1^-	5_2^-	>2.3	2.8
6_1^-	4_1^-		7.7

C. AMD results for ^{12}C

The calculations for ^{12}C with the AMD model are described in Ref. [19], where the $K^\pi = 0_1^+$ and $K^\pi = 3_1^-$ bands are constructed from triangle states with oblate deformations. In the present work, we use the same effective interactions as those for ^{28}Si.

Both of the intrinsic wave functions $\Phi_{\rm AMD}(\mathbf{Z}^{(+)})$ and $\Phi_{\rm AMD}(\mathbf{Z}^{(-)})$ for positive and negative parity show equilateral triangle shapes because of the 3α structure. As seen in density distributions shown in Figs. 2(c) and 2(d), the development of the 3α-cluster structure is more remarkable in the negative-parity intrinsic state, $\Phi_{\rm AMD}(\mathbf{Z}^{(-)})$, than in the positive-parity intrinsic state, $\Phi_{\rm AMD}(\mathbf{Z}^{(+)})$. To calculate energy levels, we perform parity and angular-momentum projections and obtain the rotational $K^\pi = 0_1^+$ and $K^\pi = 3_1^-$ bands constructed from the triangle intrinsic states, $\Phi_{\rm AMD}(\mathbf{Z}^{(+)})$ and $\Phi_{\rm AMD}(\mathbf{Z}^{(-)})$, respectively. If we tolerate the difference of the degree of the cluster development between positive- and negative-parity states, the $K^\pi = 0_1^+$ and $K^\pi = 3_1^-$ bands are roughly interpreted as the parity partners of the parity-asymmetric-intrinsic state with the triangle shape as argued in Ref. [5]. Then, we can say that the triangle shape of ^{12}C has an analogy to the pentagon shape of ^{28}Si constructing the parity partner $K^\pi = 0_1^+$ and $K^\pi = 5_1^-$ bands.

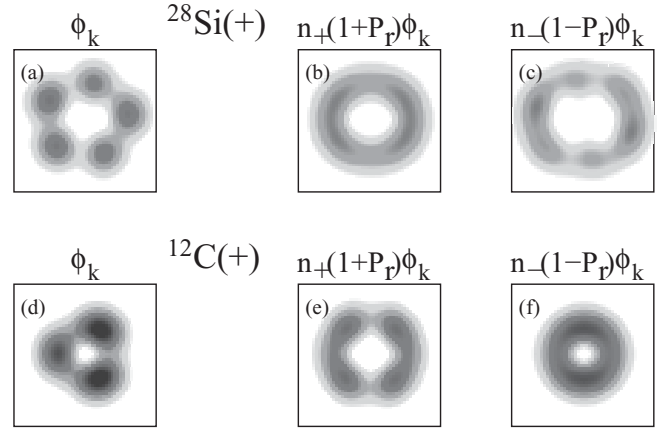

FIG. 4. (a) Density of the highest single-particle orbit $\varphi_k^{\rm HF}$ in $\Phi_{\rm AMD}(\mathbf{Z}^{(+)})$ of ^{28}Si. (b) and (c) Density for the positive- and negative-parity components of the highest orbit. Each component is normalized to be 1 by multiplying $n_p m$ with $1/n_\pm^2 = \langle\varphi_k^{\rm HF}|(1 \pm P_r)^2|\varphi_k^{\rm HF}\rangle$. (d) Density of the highest single-particle orbit in $\Phi_{\rm AMD}(\mathbf{Z}^{(+)})$ for ^{12}C. (e) and (f) Density for the positive- and negative-parity components of the highest orbit. Each component is normalized to be 1.

In a similar way to ^{28}Si, we analyze the HF single particles $\{\varphi_i^{\rm HF}\}$ in $\Phi_{\rm AMD}(\mathbf{Z}^{(+)})$ and find the parity-mixing single-particle orbits with triangular shape. The density distribution of $\varphi_i^{\rm HF}$ for the triangle shape is shown in Fig. 4(d), and those of the positive- and negative-parity components extracted from this triangle orbit are shown in Figs. 4(e) and 4(f). Both the positive- and negative-parity components show donut-shape densities, and the triangle orbit can be roughly interpreted as a linear combination $c\phi_{(0,0,\pm1)} + c'\phi_{(0,0,\mp2)}$ with $|c'|^2 \sim 0.06$ for $|c|^2 + |c'|^2 = 1$, in terms of H.O. single-particle orbits expressed by cylinder coordinates (see Appendix A). In the triangle structure of ^{12}C, a total of eight triangle orbits are found, corresponding to $c\phi_{(0,0,\pm1)} + c'\phi_{(0,0,\mp2)}$ occupied by $p\uparrow$, $p\downarrow$, $n\uparrow$, and $n\downarrow$.

III. ANALYSIS WITH BRINK-BLOCH α-CLUSTER MODELS

As described in the previous section, the pentagon and triangle shapes are found in the AMD results of ^{28}Si and ^{12}C, respectively. The AMD calculations show that these shapes originate in the 7α- and 3α-cluster features in which the α clusters are somehow dissociated because of the spin-orbit force. The AMD wave functions for the bandhead states of the $K^\pi = 0^+$ and $K^\pi = 5^-$ bands of ^{28}Si have 30% overlap with a pentagon 7α BB wave function projected onto $J^\pm = 0^+$ and 5^- states, while those of the $K^\pi = 0^+$ and $K^\pi = 3^-$ bands of ^{12}C have more than 90% overlap with a triangle 3α BB wave function projected onto $J^\pm = 0^+$ and $= 3^-$ states. The reason for the smaller overlap in ^{28}Si than that in ^{12}C is caused by the breaking of α clusters in the AMD wave functions for ^{28}Si. The fact that the 7α- and 3α-like structures are actually formed in the AMD calculation without *a priori* assuming any clusters indicates that these cluster structures are favored in ^{28}Si and ^{12}C.

The pentagon and triangle shapes are interpreted as spontaneous breaking of axial symmetry of oblate ^{28}Si and ^{12}C. In this section, to understand the mechanism of symmetry breaking, we investigate properties of ideal 7α- and 3α-cluster states by using BB α-cluster wave functions [1].

A. Brink-Bloch α-cluster wave functions

Brink-Bloch α-cluster wave functions $\Phi^{\rm BB}_{X\alpha}$ for even-even $Z = N$ nuclei with mass number $A = 4X$ are described by $X\alpha$-cluster wave functions consisting of $(0s)^4$ α clusters [1,3]. The ith α cluster is located around a certain position $\mathbf{S}_i$, and $\Phi^{\rm BB}_{X\alpha}$ is characterized by a spatial configuration of center positions of $X\alpha$ clusters, $\{\mathbf{S}_1, \ldots, \mathbf{S}_X\}$.

A BB α-cluster wave function $\Phi^{\rm BB}_{X\alpha}$ for an $X\alpha$ state can be expressed also by an AMD wave function with a specific configuration of Gaussian centers $\{\mathbf{Z}\}$. When $\mathcal{X}_i$ is chosen to be $p\uparrow$, $p\downarrow$, $n\uparrow$, and $n\downarrow$ for $i = \{1, \ldots, X\}$, $i = \{X+1, \ldots, 2X\}$, $i = \{2X+1, \ldots, 3X\}$, and $i = \{3X+1, \ldots, 4X\}$, respectively, and Gaussian centers for four nucleons ($p\uparrow$, $p\downarrow$, $n\uparrow$, $n\downarrow$) are common and real values, $\mathbf{Z}_i = \mathbf{Z}_{i+X} = \mathbf{Z}_{i+2X} = \mathbf{Z}_{i+3X} = \mathbf{S}_i/\sqrt{\nu}$ ($i = 1, \ldots, X$), the AMD wave function is equivalent to the corresponding BB α-cluster wave function for X α clusters localizing at the positions $\mathbf{S}_1, \mathbf{S}_2, \ldots, \mathbf{S}_X$.

B. Pentagon 7α Brink-Bloch wave functions

Let us consider the pentagon structure of a 7α system. The α-cluster centers $\mathbf{S}_i$ of α clusters are taken to have the pentagon configuration illustrated in Fig. 1(b) as

$$\mathbf{S}_i = \left(d\sqrt{\nu}\cos\left(\frac{2\pi}{5}i\right), d\sqrt{\nu}\sin\left(\frac{2\pi}{5}i\right), 0\right) \tag{5}$$

for $i = 1, \ldots, 5$, and

$$\mathbf{S}_i = (0, 0, \pm d'\sqrt{\nu}) \tag{6}$$

for $i = 6, 7$. Here d is the dimensionless pentagon size. Thus, the defined $\Phi^{\rm BB}_{7\alpha}$ is determined by three parameters, ν, d, and d', and hence we denote the pentagon 7α wave functions by $\Phi^{\rm BB}_{7\alpha}(\nu, d, d')$.

Next we explain the relation between $\Phi^{\rm BB}_{7\alpha}$ and shell-model wave functions by transforming the single-particle wave functions of $\Phi^{\rm BB}_{7\alpha}$ in the expansion with respect to the pentagon size d. In general, when α-cluster centers $\{\mathbf{S}_i\}$ are located around the origin, the BB wave function can be connected to a H.O. shell-model wave function by using invariance of a Slater determinant $\det\{\phi_i(\mathbf{r}_j)\} = n_0 \det\{\phi'_i(\mathbf{r}_j)\}$ under a linear transformation $\phi_i(\mathbf{r}) \to \phi'_i(\mathbf{r})$. Here n_0 is a normalization factor.

For oblate systems, we use H.O. single-particle wave functions $\phi_{(n_z,n_\rho,m_l)}$ in the expression of cylinder coordinates described in Appendix A. In the small-d' limit, the spatial wave functions for spin-up protons in $\Phi^{\rm BB}_{7\alpha}(\nu, d, d')$ can be transformed to $\det\{\phi'_i(\mathbf{r}_j)\}$, which is given by the Taylor expansion with respect to the pentagon size d as follows:

$$\begin{aligned}
\det\{\phi_{\mathbf{Z}_1}, \phi_{\mathbf{Z}_2}, \cdots, \phi_{\mathbf{Z}_7}\} &= n_0 \det\{\phi'_1, \phi'_2, \ldots, \phi'_7\},\\
\phi'_1 &= \phi_{(0,0,0)} + O(d^2),\\
\phi'_2 &= \phi_{(1,0,0)} + O(d^2),\\
\phi'_3 &= \phi_{(0,0,+1)} + O(d^2),\\
\phi'_4 &= \phi_{(0,0,-1)} + O(d^2),\\
\phi'_5 &= \phi_{(0,1,0)} + O(d^2),\\
\phi'_6 &= \phi_{(0,0,-2)} - \frac{d}{\sqrt{6}}\phi_{(0,0,+3)} + O(d^2),\\
\phi'_7 &= \phi_{(0,0,+2)} + \frac{d}{\sqrt{6}}\phi_{(0,0,-3)} + O(d^2),
\end{aligned} \tag{7}$$

where n_0 has $O(d^9, d')$. From the AMD results in Sec. II B, the typical values of d and d' are found to be $d \sim 0.5$ and $d' \sim 0.2$, resulting in only $d^2/6 = 5\%$ amplitude of the higher shell orbit ($\phi_{(0,0,+3)}$) in the next leading term. Therefore, the above expansion of the BB wave function may be reasonable for the pentagon structure of ^{28}Si. We define $\phi'^{(0)}_{1,2,3,4,5,6,7} \equiv \phi_{(0,0,0)}$, $\phi_{(1,0,0)}$, $\phi_{(0,0,+1)}$, $\phi_{(0,0,-1)}$, $\phi_{(0,1,0)}$, $\phi_{(0,0,+2)}$, $\phi_{(0,0,-2)}$. In the small-d limit, single-particle orbits ϕ'_i approach $\phi'^{(0)}_i$ and the 7α wave function becomes equivalent to the following $0\hbar\omega$ shell-model wave function with $s^2_\pi s^2_\nu p^6_\pi p^6_\nu (sd)^6_\pi (sd)^6_\nu$ configuration,

$$\Phi^{\rm BB}_{7\alpha}(\nu, d', d) \to \Phi^{(0\hbar\omega)}_{7\alpha} \equiv n_0^4 \prod_{\tau\sigma} \det\left\{\phi'^{(0)}_1 \mathcal{X}_{\tau\sigma}, \ldots, \phi'^{(0)}_7 \mathcal{X}_{\tau\sigma}\right\}, \tag{8}$$

where $\tau = \{p, n\}$ and $\sigma = \{\uparrow, \downarrow\}$. In this limit, $\Phi^{(0\hbar\omega)}_{7\alpha}$ has the axial symmetric oblate shape. Hereafter we consider only the small-d' limit and investigate properties of $\Phi^{\rm BB}_{7\alpha}(\nu, d, d')$ as functions of ν and d, $\Phi^{\rm BB}_{7\alpha}(\nu, d)$. In particular, the symmetry breaking of the oblate shape caused by finite d is discussed.

Let us consider the pentagon shape described by $\Phi^{\rm BB}_{7\alpha}$ with a finite pentagon size d. As the pentagon size d increases, the pentagon shape develops and the axial symmetry breaking of the oblate state enlarges. The leading terms of the deviation from $\Phi^{(0\hbar\omega)}_{7\alpha}$ are contained in ϕ'_6 and ϕ'_7. The orbits ϕ'_6 and ϕ'_7 are the parity-mixed orbits, and they show density with the pentagon shape as expressed in the following explicit form of the density:

$$\begin{aligned}
\phi'^*_6(\mathbf{r})\phi'_6(\mathbf{r}) &= \phi'^*_7(\mathbf{r})\phi'_7(\mathbf{r})\\
&= \frac{1}{2(\pi b^2)^{3/2}}\left(\frac{\rho}{b}\right)^4 e^{-r^2/b^2}\\
&\quad\times\left(1 + \frac{d}{3\sqrt{2}}\frac{\rho}{b}\cos(5\phi) + O(d^2)\right).
\end{aligned} \tag{9}$$

The second term, $\cos(5\phi)$, gives the density oscillation with a wave number five along the edge of the oblate shape and shows the pentagon feature. The orbits ϕ'_6 and ϕ'_7 are given by linear combinations of $\phi_{(0,0,\mp 2)}$ and $\phi_{(0,0,\pm 3)}$. Due to the mixing of $\phi_{(0,0,\pm 3)}$ in $\phi_{(0,0,\mp 2)}$ of amplitude $d^2/6$, the density of these orbits changes from the axial symmetric density to the oscillating density. This is nothing but the symmetry breaking of the rotational invariance around the z axis. If

we associate the rotational invariance with the translational invariance of uniform matter, and the z-component of the angular momentum m_l with the momentum k, then we find a good correspondence of the ϕ'_6 and ϕ'_7 orbits with the single-particle wave functions of the nuclear matter DW proposed by Overhauser [12]. In other words, the pentagon shape can be interpreted as the static DW at the edge of the oblate state. As shown below, $\Phi^{\rm BB}_{7\alpha}(\nu, d)$ is expressed by coherent particle-hole configurations from $\Phi^{(0\hbar\omega)}_{7\alpha}$.

We show the particle-hole representation of $\Phi^{\rm BB}_{7\alpha}(\nu, d)$ below. We assume that $\Phi^{(0\hbar\omega)}_{7\alpha}$ is the Hartree-Fock vacuum $|0\rangle_{\rm F}$, and $\phi_{(0,0,\pm3)}\mathcal{X}_{\tau\sigma}$ and $\phi_{(0,0,\pm2)}\mathcal{X}_{\tau\sigma}$ are the levels above and below the Fermi level, respectively. We define the particle and hole operators as

$$a^\dagger_{\pm k,\tau\sigma} = c^\dagger_{\pm k,\tau\sigma}, \quad b^\dagger_{\pm q,\tau\sigma} = c_{\mp q,\tau-\sigma}, \tag{10}$$

where the labels $k \equiv 3$ and $q \equiv 2$ indicate m_l for particles and holes. When higher order terms, $O(d^2)$, in the single-particle wave functions ϕ' are ignored, $\Phi^{\rm BB}_{7\alpha}(\nu, d)$ can be approximated to be

$$\Phi^{\rm BB}_{7\alpha}(\nu, d) \approx \prod_\chi \left(1 + \frac{d}{\sqrt{6}} a^\dagger_{-k,\chi} b^\dagger_{-q,-\chi}\right) \times \left(1 - \frac{d}{\sqrt{6}} a^\dagger_{+k,\chi} b^\dagger_{+q,-\chi}\right)|0\rangle_{\rm F}, \tag{11}$$

with $\chi = \tau\sigma$ and $-\chi = \tau - \sigma$. As clearly seen, the product of the particle and hole operators, $a^\dagger_{\pm k,\chi} b^\dagger_{\pm q,-\chi}$, brings quanta $K = \pm 5$.

C. Triangle 3α Brink-Bloch wave functions

In a similar way to the pentagon 7α state $\Phi^{\rm BB}_{7\alpha}(\nu, d)$, the equilateral triangle 3α state is related to axial symmetry breaking of the oblate state in the p shell, and the triangle shape is described by parity-mixed orbits. In the BB α-cluster wave function $\Phi^{\rm BB}_{3\alpha}$ for the 3α structure, the parameters $\mathbf{S}_i$ $(i = 1, \ldots, 3)$ with a triangle configuration are written as

$$\mathbf{S}_i = \left(d\sqrt{\nu}\cos\left(\frac{2\pi}{3}i\right), d\sqrt{\nu}\sin\left(\frac{2\pi}{3}i\right), 0\right). \tag{12}$$

$\Phi^{\rm BB}_{3\alpha}$ is specified by the parameters ν, d as $\Phi^{\rm BB}_{3\alpha}(\nu, d)$, where d is the dimensionless triangle size. With a proper transformation $\phi_{\mathbf{Z}_i}(\mathbf{r}) \to \phi'_i(\mathbf{r})$ and a Taylor expansion of the transformed single-particle orbits $\phi'_i(\mathbf{r})$ with respect to the triangle size d, we can rewrite the spatial wave function for three identical nucleons,

$$\det\{\phi_{\mathbf{Z}_1}, \phi_{\mathbf{Z}_2}, \phi_{\mathbf{Z}_3}\} = n_0 \det\{\phi'_1, \phi'_2, \phi'_3\}, \tag{13}$$

with

$$\begin{aligned} \phi'_1 &= \phi'^{(0)}_1, \\ \phi'_2 &= \phi'^{(0)}_2 + \frac{d}{2}\phi_{(0,0,+2)} + O(d^2), \\ \phi'_3 &= \phi'^{(0)}_3 - \frac{d}{2}\phi_{(0,0,-2)} + O(d^2), \end{aligned} \tag{14}$$

where

$$\begin{aligned} \phi'^{(0)}_1 &\equiv \phi_{(0,0,0)}, \\ \phi'^{(0)}_2 &\equiv \phi_{(0,0,-1)}, \\ \phi'^{(0)}_3 &\equiv \phi_{(0,0,+1)}. \end{aligned} \tag{15}$$

In the small-d limit, $\Phi^{\rm BB}_{3\alpha}(\nu, d)$ becomes equivalent to the $0\hbar\omega$ shell-model wave function,

$$\begin{aligned} \Phi^{\rm BB}_{3\alpha}(\nu, d) &\to n_0^4 \Phi^{(0\hbar\omega)}_{3\alpha}, \\ \Phi^{(0\hbar\omega)}_{3\alpha} &\equiv \prod_{\tau\sigma} \det\{\phi'^{(0)}_1 \mathcal{X}_{\tau\sigma}, \ldots, \phi'^{(0)}_3 \mathcal{X}_{\tau\sigma}\}. \end{aligned} \tag{16}$$

The orbits ϕ'_2 and ϕ'_3 are the parity-mixed orbits, and their density shows a triangle shape with the form

$$\begin{aligned} \phi'^*_2(\mathbf{r})\phi'_2(\mathbf{r}) &= \phi'^*_3(\mathbf{r})\phi'_3(\mathbf{r}) \\ &= \frac{1}{(\pi b^2)^{3/2}} \left(\frac{r}{b}\right)^2 e^{-r^2/b^2} \\ &\quad \times \left(1 + \frac{d}{2\sqrt{2}} \frac{r}{b} \cos(3\phi) + O(d^2)\right). \end{aligned} \tag{17}$$

Similarly to the particle-hole representation of the 7α wave function, $\Phi^{\rm BB}_{3\alpha}(\nu, d)$ of order d can be written in the particle-hole representation by using alternative definitions $k \equiv 2, q \equiv 1$, and $|0\rangle_{\rm F} \equiv \Phi^{(0\hbar\omega)}_{3\alpha}(\nu, d)$,

$$\Phi^{\rm BB}_{3\alpha}(\nu, d) \approx \prod_\chi \left(1 - \frac{d}{2} a^\dagger_{-k,\chi} b^\dagger_{-q,-\chi}\right) \times \left(1 + \frac{d}{2} a^\dagger_{+k,\chi} b^\dagger_{+q,-\chi}\right)|0\rangle_{\rm F}. \tag{18}$$

D. Development of the 7α and 3α states

We calculate energies of the 7α pentagon state $\Phi^{\rm BB}_{7\alpha}(\nu, d)$ and the 3α triangle state $\Phi^{\rm BB}_{3\alpha}(\nu, d)$ as functions of ν and d. The energies are evaluated by calculating expectation values of the Hamiltonian $H_{\rm eff}$ given in Sec. II A with respect to the intrinsic state $\Phi^{\rm BB}_{7\alpha}(\nu, d)$, and also the positive-parity projected state $(1 + P_r)\Phi^{\rm BB}_{7\alpha}(\nu, d)$, the negative-parity projected state $(1 - P_r)\Phi^{\rm BB}_{7\alpha}(\nu, d)$, and the $K^\pi = 0^+$ projected one $P^{K=0}(1 + P_r)\Phi^{\rm BB}_{7\alpha}(\nu, d)$. The parity projection corresponds to the restoration of the broken parity symmetry of the intrinsic state, and the $K = 0$ projection restores the broken axial symmetry. The energy minimum state of $P^{K=0}(1 + P_r)\Phi^{\rm BB}_{7\alpha}(\nu, d)$ may relate to the structure of the $K^\pi = 0^+_1$ band in ^{28}Si, while that of $(1 - P_r)\Phi^{\rm BB}_{7\alpha}(\nu, d)$ corresponds to the $K^\pi = 5^-_1$ band because $(1 - P_r)\Phi^{\rm BB}_{7\alpha}(\nu, d)$ is equivalent to the $K^\pi = 5^-$ projected state at least in case of small d. Note that the projected states may contain higher correlations beyond a single Slater determinant.

The contour plots of energy surfaces are shown in Fig. 5 as functions of ν and $d^2/6$. It is found that the energy minimum of the energy surface for $\Phi^{\rm BB}_{7\alpha}(\nu, d)$ with no projection is located at $d^2/6 \sim 0.1$. The finite pentagon size d of the energy minimum indicates the development of pentagon shape, namely, the spontaneous breaking of axial symmetry in the intrinsic structure. As seen in the minima of the energy

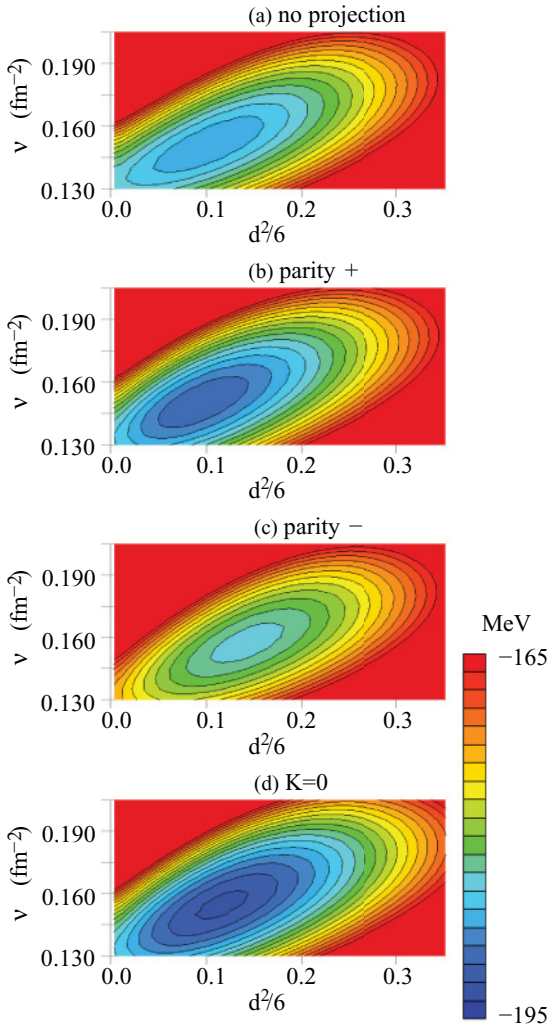

FIG. 5. (Color online) (a) Energy expectation values of $\Phi^{\rm BB}_{7\alpha}(\nu, d)$ plotted as functions of $d^2/6$ and ν. (b), (c), and (d) Energy expectation values of the positive-parity state, the negative-parity state, and the $K = 0$ state projected from the intrinsic wave function $\Phi^{\rm BB}_{7\alpha}(\nu, d)$. The parameter d' is taken to be a small value, $d'/\sqrt{\nu} = 0.1$ fm.

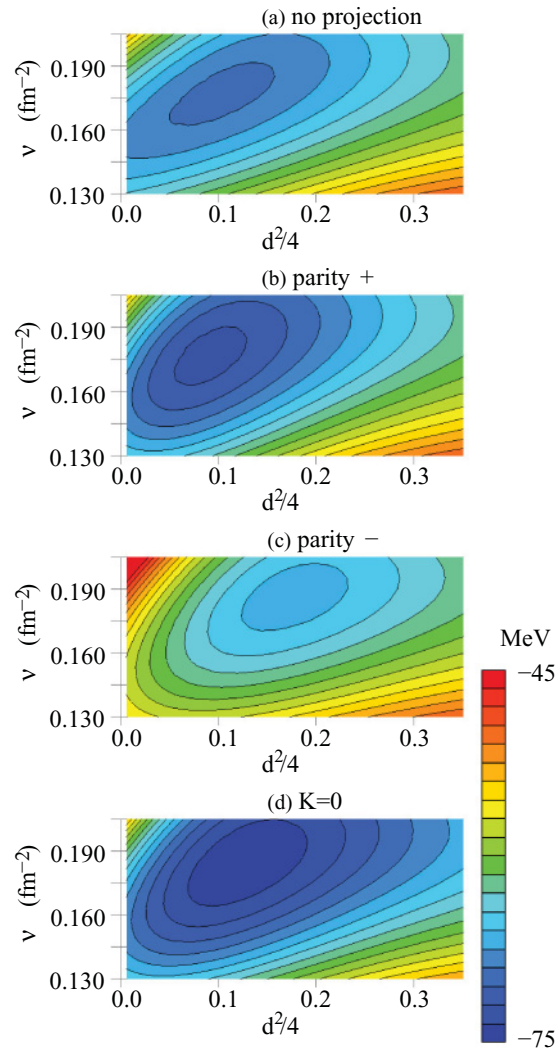

FIG. 6. (Color online) (a) Energy expectation values of $\Phi^{\rm BB}_{3\alpha}(\nu, d)$ plotted as functions of $d^2/4$ and ν. (b), (c), and (d) Energy expectation values of the positive-parity state, the negative-parity state, and the $K = 0$ state projected from the intrinsic wave function $\Phi^{\rm BB}_{3\alpha}(\nu, d)$. The parameter d' is taken to be a small value, $d'/\sqrt{\nu} = 0.1$ fm.

surfaces shown in Figs. 5(d) and 5(c), the development of the pentagon shape is enhanced in the $K^\pi = 0^+$ projected state, and it is largest in the negative-parity projected state.

The value $d^2/6$ indicates approximately the mixing amplitude of the negative-parity component in the pentagon orbits, ϕ'_6 and ϕ'_7, as given in Eq. (7). The value $d^2/6 \sim 0.1$ at the energy minimum of the positive-parity projected state indicates ∼10% mixing, which is comparable to 5% mixing of the negative-parity component in the pentagon orbits in the AMD wave function $\Phi_{\rm AMD}(\mathbf{Z}^+)$ for ^{28}Si. The main reason for the smaller mixing in the AMD result than that in the ideal 7α-cluster model may be α-cluster dissociation effects in the AMD calculations.

We also calculate the energy of the equilateral triangle 3α state $\Phi^{\rm BB}_{3\alpha}(\nu, d)$ as functions of ν and d. Energies are calculated with respect to the intrinsic state $\Phi^{\rm BB}_{3\alpha}(\nu, d)$, the positive-parity projected state $(1 + P_r)\Phi^{\rm BB}_{3\alpha}(\nu, d)$, the negative-parity projected state $(1 - P_r)\Phi^{\rm BB}_{3\alpha}(\nu, d)$, and the $K^\pi = 0^+$ projected one $P^{K=0}(1 + P_r)\Phi^{\rm BB}_{3\alpha}(\nu, d)$. The energy minimum state of $P^{K=0}(1 + P_r)\Phi^{\rm BB}_{3\alpha}(\nu, d)$ describes the structure of the $K^\pi = 0^+_1$ band in ^{12}C, while that of $(1 - P_r)\Phi^{\rm BB}_{3\alpha}(\nu, d)$ corresponds to the $K^\pi = 3^-_1$ band.

The contour plots of the energy surfaces are shown in Fig. 6 as functions of ν and $d^2/4$. $d^2/4$ is approximately the mixing amplitude of $\phi_{0,0,\mp 2}$ in $\phi_{0,0,\pm 1}$ as described in Eq. (13). The finite $d^2/4$ value of the energy minimum indicates the development of a 3α-cluster structure. The energy minimum of the energy surface for $\Phi^{\rm BB}_{3\alpha}(\nu, d)$ with no projection is located at $d^2/4 \sim 0.1$. The cluster development is slightly enhanced in the $K^\pi = 0^+$ projected state, and it is most remarkable in the negative-parity projected state. This is consistent with the AMD calculations of ^{12}C shown in Fig. 2. One of the interesting features of $\Phi^{\rm BB}_{3\alpha}(\nu, d)$ is that the energy surface is

quite shallow against the large triangle size d at $\nu \sim 0.20$. This corresponds to 3α-cluster breakup.

E. Roles of the parity and K^π projections in a mean-field picture

As mentioned before, in the particle-hole representation based on $|\Phi^{(0\hbar\omega)}_{7\alpha}\rangle = |0\rangle_{\rm F}$, $\Phi^{\rm BB}_{7\alpha}(\nu, d)$ can be approximately expressed as Eq. (11). At least in the order d, the negative-parity projected state is nothing but a linear combination of 1p-1h states,

$$(1 - P_r)\left|\Phi^{\rm BB}_{7\alpha}(\nu, d)\right\rangle \approx \frac{d}{\sqrt{6}} \sum_{\chi} (a^\dagger_{-k,\chi} b^\dagger_{-q,-\chi} - a^\dagger_{+k,\chi} b^\dagger_{+q,-\chi})|0\rangle_{\rm F}. \quad (19)$$

Thus, $(1 - P_r)\Phi^{\rm BB}_{7\alpha}(\nu, d)$ is described by the coherent sum of the 1p-1h states, $a^\dagger_{-k,\chi} b^\dagger_{-q,-\chi}|0\rangle_{\rm F}$ and $a^\dagger_{+k,\chi} b^\dagger_{+q,-\chi}|0\rangle_{\rm F}$. This indicates that the negative-parity state can be described by the $K^\pi = 5^-$ vibration mode of the oblate shape. This is an alternative interpretation of the $K^\pi = 5^-$ band. However, as already discussed, since the axial symmetry of the oblate state is already broken in the intrinsic state before the negative-parity projection (see Fig. 5), the $K^\pi = 5^-$ band is regarded as the static pentagon "shape" instead of the $K^\pi = 5^-$ vibration of the oblate state.

The positive-parity projected state corresponds to the mixing of 2p-2h states having $K = 0$ and $K = \pm 10$ into the dominant $\Phi^{(0\hbar\omega)}_{7\alpha}$ state. The high K components do not affect the $K^\pi = 0^+$ ground band, and actually they are dropped in the $K = 0$ projection. Consequently, the $K^\pi = 0^+$ projected state contains only the 2p-2h states with $K = 0$,

$$P^{K=0}(1 + P_r)\left|\Phi^{\rm BB}_{7\alpha}(\nu, d)\right\rangle \approx |0\rangle_{\rm F} - \frac{d^2}{6} \sum_{\chi} \sum_{\chi'} a^\dagger_{-k,\chi} b^\dagger_{-q,-\chi} a^\dagger_{+k,\chi'} b^\dagger_{+q,-\chi'}|0\rangle_{\rm F}. \quad (20)$$

The contained 2p-2h states are k and $-k$ particle pairs and q and $-q$ hole pairs, and they are associated with Cooper pairs in BCS theory [24]. Let us remind the reader that the normal pairings in nuclear systems are considered to be neutron-neutron pairing and proton-proton pairing in the spin $S = 0$ channel. However, the 2p-2h terms in Eq. (20) have not only spin-zero nn and pp pairs but also spin-one np pairs. Namely, an $(S, T) = (1, 0)$ (spin-one isoscalar) particle-particle pair and an $(S, T) = (1, 0)$ hole-hole pair couple to be totally $S = 0$ and $T = 0$, while an $(S, T) = (0, 1)$ (spin-zero isovector) particle-particle pair and an $(S, T) = (0, 1)$ hole-hole pair couple to be $S = 0$ and $T = 0$. Because of the large number of coherent pairs, the $K^\pi = 0^+$ state projected from the 7α-cluster state may gain much correlation energy.

In these analyses, we can say that, in both the negative-parity and $K^\pi = 0^+$ states, the coherent particle-hole configurations due to the coherent edge DWs of four kinds, $\chi = p\uparrow$, $p\downarrow$, $n\uparrow$, and $n\downarrow$, play an important role in the development of the pentagon shape. We will show the importance of the coherence for SSB in later sections.

IV. EXTENSION OF BRINK-BLOCH α-CLUSTER MODELS

As discussed in the previous section, the coherent proton and neutron edge DWs are essential to develop the pentagon and triangle shapes. In this section, we investigate the development of the pentagon and triangle shapes without the proton-neutron coherence by considering a pentagon or triangle neutron structure with a frozen proton structure. Toward this aim, we extend the BB α-cluster wave functions for the pentagon 7α- and the triangle 3α-cluster states as follows: We assume the pentagon configurations of proton and neutron structures for a $Z = N = 14$ system but take the pentagon size d in Eq. (5) independently for protons and neutrons. We take a small enough value of the pentagon size d_p for protons and vary the size d_n for neutrons. Thus, the defined wave function can be written in an expansion of order d_n as

$$\begin{aligned}
&\Phi_{7\alpha-n}(\nu, d_n) \\
&\quad \approx n'_0 \prod_\sigma \det\left\{\phi'^{(0)}_1 \mathcal{X}_{p\sigma}, \ldots, \phi'^{(0)}_7 \mathcal{X}_{p\sigma}\right\} \prod_\sigma \det \\
&\quad \times \left\{\phi'^{(0)}_1 \mathcal{X}_{n\sigma}, \ldots, \phi'^{(0)}_5 \mathcal{X}_{n\sigma}, \phi'_6 \mathcal{X}_{n\sigma}, \phi'_7 \mathcal{X}_{n\sigma}\right\}, \\
&\quad \phi'_6 = \phi_{(0,0,-2)} - \frac{d_n}{\sqrt{6}} \phi_{(0,0,+3)} + O\left(d_n^2\right), \\
&\quad \phi'_7 = \phi_{(0,0,+2)} + \frac{d_n}{\sqrt{6}} \phi_{(0,0,-3)} + O\left(d_n^2\right). \qquad (21)
\end{aligned}$$

In a similar way, we also assume the triangle configurations of proton and neutron structures for a $Z = N = 6$ system by taking the triangle size d in Eq. (12) independently for protons and neutrons. We take a small enough value of the triangle size d_p for protons and vary the size d_n for neutrons. Then the wave function can be written in an expansion of order d_n as

$$\begin{aligned}
\Phi_{3\alpha-n}(\nu, d_n) &\approx n'_0 \prod_\sigma \det\left\{\phi'^{(0)}_1 \mathcal{X}_{p\sigma} \phi'^{(0)}_2 \mathcal{X}_{p\sigma} \phi'^{(0)}_3 \mathcal{X}_{p\sigma}\right\} \\
&\quad \times \prod_\sigma \det\left\{\phi'^{(0)}_1 \mathcal{X}_{n\sigma} \phi'_2 \mathcal{X}_{n\sigma} \phi'_3 \mathcal{X}_{n\sigma}\right\}, \\
\phi'_2 &= \phi'^{(0)}_2 + \frac{d_n}{2} \phi_{(0,0,+2)} + O\left(d_n^2\right), \\
\phi'_3 &= \phi'^{(0)}_3 - \frac{d_n}{2} \phi_{(0,0,-2)} + O\left(d_n^2\right). \qquad (22)
\end{aligned}$$

Moreover, we consider the triangle proton structure in a $Z = 6$ and $N = 14$ system to study the proton edge DW in a neutron-rich system. For the frozen neutron structure, we adopt a pentagon configuration for the neutron part with a small enough pentagon size d_n. The proton structure is assumed to be a triangle structure with triangle size d_p, which is a variational parameter. The wave function can be written in an expansion of order d_p as

$$\begin{aligned}
\Phi_{^{20}\mathrm{C}\text{-}p}(\nu, d_p) &\approx n'_0 \prod_{\sigma=\{\uparrow,\downarrow\}} \det\left\{\phi'^{(0)}_1 \mathcal{X}_{p\sigma}, \phi'_2 \mathcal{X}_{p\sigma}, \phi'_3 \mathcal{X}_{p\sigma}\right\} \\
&\quad \times \prod_{\sigma=\{\uparrow,\downarrow\}} \det\left\{\phi'^{(0)}_1 \mathcal{X}_{n\sigma}, \ldots, \phi'^{(0)}_7 \mathcal{X}_{n\sigma}\right\}, \\
\phi'_2 &= \phi'^{(0)}_2 + \frac{d_p}{2} \phi_{(0,0,+2)} + O\left(d_p^2\right), \\
\phi'_3 &= \phi'^{(0)}_3 - \frac{d_p}{2} \phi_{(0,0,-2)} + O\left(d_p^2\right). \qquad (23)
\end{aligned}$$

This model corresponds to a 3α core structure in the ^{20}C system.

We calculate energies of $\Phi_{7\alpha-n}(\nu, d_n)$, $\Phi_{3\alpha-n}(\nu, d_n)$, and $\Phi_{^{20}\mathrm{C}\text{-}p}(\nu, d_p)$ states and compare the results with $\Phi^{\mathrm{BB}}_{7\alpha}(\nu, d)$ and $\Phi^{\mathrm{BB}}_{3\alpha}(\nu, d)$. The energies are evaluated by calculating expectation values of the effective Hamiltonian H_{eff} for these states with no projection, the positive- and negative-parity projected states, and the $K^\pi = 0^+$ projected states.

At first, we compare the pentagon size dependence of the energies of $\Phi_{7\alpha\text{-}n}(\nu, d_n)$ having a frozen proton structure with that of $\Phi^{\mathrm{BB}}_{7\alpha}(\nu, d)$ having proton-neutron coherent pentagon shapes. The energy curves are shown in Fig. 7. In each system, ν is fixed to be the optimum value at the energy minimum solution in the ν-d plane for the positive-parity projected state. As already discussed in the previous section, $\Phi^{\mathrm{BB}}_{7\alpha}(\nu, d)$ shows a deep energy pocket around the energy minimum at a finite d value [see Fig. 7(a)]. This indicates the development of the pentagon shape, which corresponds to the spontaneous breaking of the axial symmetry of the oblate state $\Phi^{(0\hbar\omega)}_{7\alpha}$. The potential pockets are deeper in the projected states than in the intrinsic state with no projection. In contrast to the energy curve for $\Phi^{\mathrm{BB}}_{7\alpha}(\nu, d)$, the energy curve for $\Phi_{7\alpha\text{-}n}(\nu, d_n)$ with no projection has a minimum around $d_n = 0$, which corresponds to the axial symmetric oblate state $\Phi^{(0\hbar\omega)}_{7\alpha}$. Even in the projected states, there is no deep pocket in a finite d_n region, and the pentagon shape of the neutron structure is suppressed in the frozen proton structure. This means that the neutron edge DW on the oblate state $\Phi^{(0\hbar\omega)}_{7\alpha}$ does not occur without the coherent proton edge DW. This may lead to suppression of the pentagon shape in $Z \neq N$ nuclei.

Next we discuss the triangle structures in $Z = 6$ nuclei. In a similar way to the pentagon structure, we compare the triangle size dependence of the energies of $\Phi_{3\alpha\text{-}n}(\nu, d_n)$ having a frozen proton structure with that of $\Phi^{\mathrm{BB}}_{3\alpha}(\nu, d)$ having proton-neutron coherent triangle shapes in Figs. 8(a) and 8(b). Again we find that each energy curve for $\Phi_{3\alpha\text{-}n}(\nu, d_n)$ has a minimum around $d_n = 0$, which corresponds to $\Phi^{(0\hbar\omega)}_{3\alpha}$. This is in contrast to the features of $\Phi^{\mathrm{BB}}_{3\alpha}(\nu, d)$, which shows a deep energy pocket at a finite d, indicating the developed triangle shape. We also consider the proton triangle shape in the $Z = 6, N = 14$ system, $\Phi_{^{20}\mathrm{C}\text{-}p}(\nu, d_p)$. The finite d_p corresponds to the development of the 3α core structure in the ^{20}C system with oblate proton and neutron structures. The energy of $\Phi_{^{20}\mathrm{C}\text{-}p}(\nu, d_p)$ is smallest around $d = 0$ and increases as the triangle size d_p becomes large. Compared with the energy curve of $\Phi_{3\alpha\text{-}n}(\nu, d_n)$, the triangle proton structure is significantly unfavored in the $Z = 6, N = 14$ system.

We conclude that the proton-neutron coherence is essential in the development of the pentagon and triangle structures of the oblate states in $Z = N$ nuclei. Needless to say, this is consistent with the cluster aspect of $Z = N$ nuclei. In the oblate state of neutron-rich C, the triangle cluster structure is suppressed. The first reason for the quenching of cluster structure is the lack of proton-neutron coherence. The second reason is the expanded level spacing of proton orbits in neutron-rich nuclei because protons are deeply bound due to excess neutrons. Since the energy cost for 1p-1h proton excitations increases in the neutron-rich system, the correlation energy due to the triangle structure may not be able to overcome the cost. We shall discuss the details in the next section.

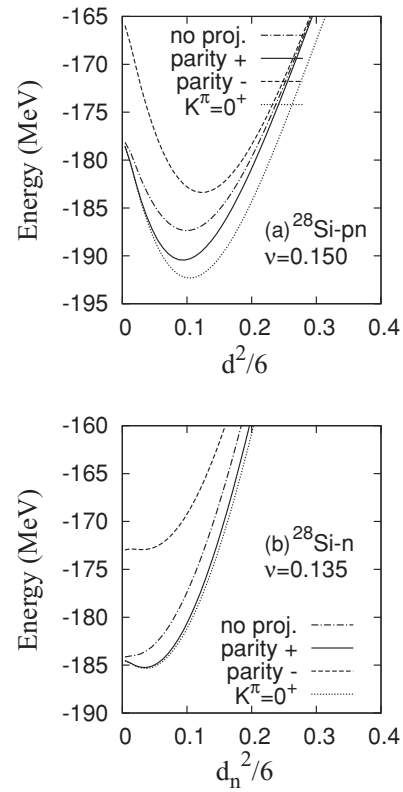

FIG. 7. (a) The energy of the 7α state $\Phi^{\mathrm{BB}}_{7\alpha}(\nu, d)$ as a function of $d^2/6$. d is the pentagon size for protons and neutrons. (b) The energy of the $Z = N = 14$ state $\Phi_{7\alpha\text{-}n}(\nu, d_n)$ with the frozen proton structure as a function of $d_n^2/6$. d_n is the pentagon size for neutrons. In each system, ν is fixed to be the optimum value at the energy minimum solution in the ν-d plane for the positive-parity projected states as (a) $\nu = 0.15\ \mathrm{fm}^{-2}$ and (b) $\nu = 0.135\ \mathrm{fm}^{-2}$. The parameter d' is chosen to be $d'/\sqrt{\nu} = 0.1$ fm.

V. EDGE DENSITY WAVE AND SPONTANEOUS SYMMETRY BREAKING

As already mentioned, the pentagon and triangle structures can be interpreted as the static edge DWs at the surface of the oblate states, which is expected to connect with the spontaneous symmetry breaking of rotational invariance around the symmetric axis.

Systems with strong interaction exhibit various SSB phenomena such as nuclear BCS, chiral symmetry breaking, and color superconductivities. These SSB phenomena occur both homogeneously and inhomogeneously. In particular, inhomogeneous SSB phases are discussed in the framework of nuclear DWs, chiral DWs, and Fulde-Ferrel-Larkin-Ovchinnikov states in the color superconducting phase [12,25–39], whose phase breaks translational invariance and whose corresponding

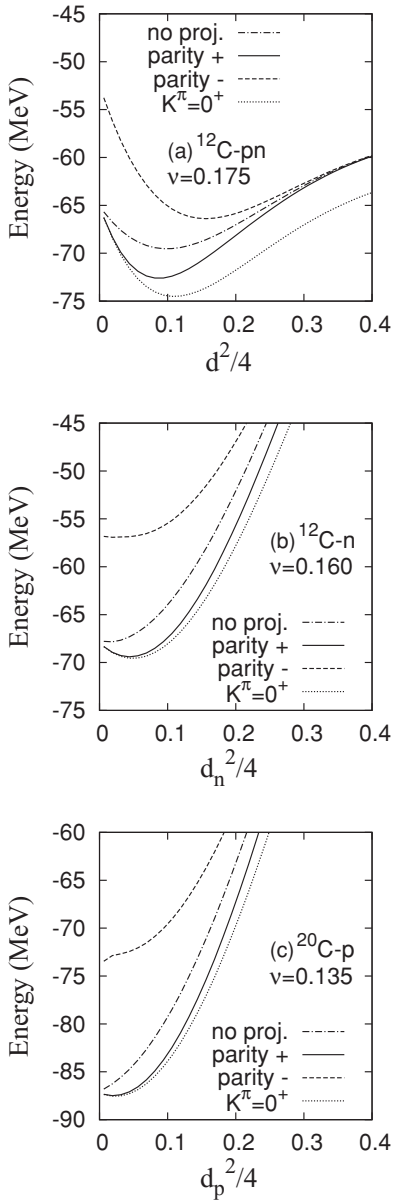

FIG. 8. (a) The energy of the 3α state $\Phi^{\rm BB}_{3\alpha}(\nu, d)$ as a function of $d^2/4$, where d is the pentagon size for protons and neutrons. (b) The energy of the $Z = N = 6$ state $\Phi_{3\alpha\text{-}n}(\nu, d_n)$ with the frozen proton structure as a function of $d_n^2/4$. d_n is the pentagon size for neutrons. (c) The energy of the $Z = 6$, $N = 14$ system $\Phi_{^{20}\text{C-p}}(\nu, d_p)$ with the frozen proton structure. The pentagon size d_n for the frozen neutron structure is taken to be $d_n^2 = 0.025$. In each system, ν is fixed to be the optimum value at the energy minimum solution in the ν-d plane for the positive-parity projected states as (a) $\nu = 0.175$ fm^{-2}, (b) $\nu = 0.160$ fm^{-2}, and (c) $\nu = 0.135$ fm^{-2}.

condensation operator depends on the spatial coordinates. More generally, SSB resulting in a spatially nonuniform vacuum relates to condensation operators with finite momenta. When we understand nuclear matter DW as the instability of the Fermi surface, the condensation operator is given in the form $a^\dagger_{k_F} b^\dagger_{k_F}$, which has momentum $2k_F$ (where k_F is the Fermi momentum). In condensed matter physics, inhomogeneous phases with DWs are discussed as charge DWs and spin DWs [40,41].

These phenomena in infinite systems are discussed in terms of the order parameters, which are characterized by nonzero expectation values of certain operators. In finite systems, however, the symmetry cannot be broken in the energy eigenstates, because the symmetry is restored even if it is broken in the intrinsic state. Nevertheless, it is useful to discuss SSB in the state before projection or restoration by analyzing expectation values of specific operators resembling the condensation operators as done for the BCS phenomena in finite nuclei. For the pentagon and triangle structures, the expressions in Eqs. (11) and (18) are of a form similar to the matter DW operators $a^\dagger_{k_F} b^\dagger_{k_F}$.

In this section, we describe SSB for edge DWs by introducing a simplified model in Appendix C, and we discuss the development and suppression of the pentagon and triangle structures from the viewpoint of the edge DWs. In this model, $\Phi^{(0\hbar\omega)}_{7\alpha}$ is assumed to be the Hartree-Fock vacuum $|0\rangle_{\rm F}$, and the orbits $|\phi_{(0,0,\pm q)}\mathcal{X}_{\tau\sigma}\rangle$ and $|\phi_{(0,0,\pm k)}\mathcal{X}_{\tau\sigma}\rangle$ are considered to be active Hartree-Fock single-particle states. This means that the model space is truncated within $\phi_{(0,0,\pm k)}\mathcal{X}_{\tau\sigma}$ for particle states and $\phi_{(0,0,\pm q)}\mathcal{X}_{\tau\sigma}$ for hole states. This is equivalent to a model of 8 particles for 16 states, which is a kind of half-filled model. For the residual interaction, we assume a contact interaction and adopt $H_{\rm DW}$ defined in Eq. (C7). Note that this model is applicable also to the 3α oblate state by replacing $q = 2$ and $k = 3$ for the 7α state with $q = 1$ and $k = 2$. Then, the Hamiltonian in the particle-hole representation can be written as

$$\begin{aligned}
H &= H_0 + H_1 + H_{\rm DW},\\
H_0 &= {}_{\rm F}\langle 0|H|0\rangle_{\rm F},\\
H_1 &= \sum_\chi E_{k,\tau} a^\dagger_{+k,\chi} a_{+k,\chi} + \sum_\chi E_{k,\tau} a^\dagger_{-k,\chi} a_{-k,\chi}\\
&\quad - \sum_\chi E_{q,\tau} b^\dagger_{+q,\chi} b_{+q,\chi} - \sum_\chi E_{k,\tau} b^\dagger_{-q,\chi} b_{-q,\chi},\\
H_{\rm DW} &= 2\sum_{\chi,\chi'} G^{(ph)}_{\chi,\chi'} [a^\dagger_{+k,\chi} b^\dagger_{+q,-\chi} b_{+q,-\chi'} a_{+k,\chi'}\\
&\quad + a^\dagger_{-k,\chi} b^\dagger_{-q,-\chi} b_{-q,-\chi'} a_{-k,\chi'}].
\end{aligned} \tag{24}$$

Here $\chi = \tau\sigma$ and $-\chi = \tau - \sigma$.

We use an ansatz for the new vacuum of the edge DWs with axial-symmetry breaking as

$$\begin{aligned}
|\Psi\rangle &= \prod_\chi (v_\tau + u_\tau a^\dagger_{+k,\chi} b^\dagger_{+q,-\chi})\\
&\quad \times \prod_\chi (v^*_\tau - u^*_\tau a^\dagger_{-k,\chi} b^\dagger_{-q,-\chi})|0\rangle_{\rm F},
\end{aligned} \tag{25}$$

with

$$|v_\tau|^2 + |u_\tau|^2 = 1, \tag{26}$$

where v_τ and u_τ are variational parameters determined by the energy variation, and time reversal invariance is taken into account. Our ansatz, Eq. (25), has the same form as that obtained in the approximation that the quantum fluctuation of

the particle-hole operators such as $a^\dagger_{\pm k,\chi} b^\dagger_{\pm q,-\chi}$ are omitted, as shown in Appendix D. It is clear that Ψ is equivalent to $\Phi^{\rm BB}_{7\alpha}(\nu, d)$ with $u_\tau = -d/\sqrt{6}$ in the order d approximation given by Eq. (11) [or $\Phi^{\rm BB}_{3\alpha}(\nu, d)$ with $u_\tau = d/2$]. In general, the coefficients u_τ and v_τ are complex. The phase ϕ_0 of u_τ/v_τ corresponds to the constant shift of the rotation angle $\phi \to \phi + \phi_0$ in the density oscillation $\cos(5\phi)$ in Eq. (9). Since the phase ϕ_0 for the lowest-energy solution is isospin independent, hereafter, u_τ and v_τ are taken to be real quantities. The expectation values for this vacuum $|\Psi\rangle$ are

$$\begin{aligned} \langle a^\dagger_{\pm k,\chi} a_{\pm k,\chi}\rangle &= \langle b^\dagger_{\pm q,-\chi} b_{\pm q,-\chi}\rangle = u_\tau u_\tau, \\ \langle a^\dagger_{\pm k,\chi} b^\dagger_{\pm q,-\chi}\rangle &= \langle b_{\pm q,-\chi} a_{\pm k,\chi}\rangle = \pm u_\tau v_\tau. \end{aligned} \tag{27}$$

The normal state $|0\rangle_{\rm F}$ has $v_\tau = 1$ and $u_\tau = 0$, while the SSB vacuum has a finite $\langle a^\dagger_{\pm k,\chi} b^\dagger_{\pm q,-\chi}\rangle$, i.e., a finite value of $u_\tau v_\tau$.

The values v_τ and u_τ are determined by minimizing the expectation value $\langle\Psi|H|\Psi\rangle$,

$$\begin{aligned} E &= \langle\Psi|H|\Psi\rangle = H_0 + 2E_{\rm corr}, \\ E_{\rm corr} &= \sum_{\tau\sigma}(E_{k,\tau} - E_{q,\tau})u^2_\tau + 2\sum_{\chi,\chi'} G^{(ph)}_{\chi,\chi'} u_\tau v_\tau u_{\tau'} v_{\tau'}. \end{aligned} \tag{28}$$

For $Z = N$ systems, when isospin dependencies of single-particle energies $E_{k,\tau}$ and $E_{q,\tau}$ are ignored, v_τ and u_τ do not depend on the isospin τ, and the energy correction $E_{\rm corr}$ from the energy H_0 is

$$\begin{aligned} E_{\rm corr} &= \sum_{\tau\sigma}(E_{k,\tau} - E_{q,\tau})u^2_\tau + 2\sum_{\chi\neq\chi'} g^{(ph)} u_\tau v_\tau u_{\tau'} v_{\tau'} \\ &= 4\{(E_k - E_q)u^2 + 6g^{(ph)}u^2v^2\}. \end{aligned} \tag{29}$$

The stationary condition with respect to variations of u and v with the constraint $u\delta u + v\delta v = 0$ leads to the equation

$$(E_k - E_q)u - 6g^{(ph)}u(u^2 - v^2) = 0. \tag{30}$$

For a nonzero u, u and v are solved as follows:

$$\begin{aligned} u^2 &= \frac{1}{2}\left(1 + \frac{E_k - E_q}{6g^{(ph)}}\right), \\ v^2 &= \frac{1}{2}\left(1 - \frac{E_k - E_q}{6g^{(ph)}}\right), \\ uv &= \frac{1}{2}\sqrt{1 - \left(\frac{E_k - E_q}{6g^{(ph)}}\right)^2}. \end{aligned} \tag{31}$$

It turns out that, to obtain a nonzero uv with real u and v values for the SSB vacuum, the following condition must be satisfied:

$$E_k - E_q < -6g^{(ph)}. \tag{32}$$

This indicates that SSB occurs provided that the strength $-g^{(ph)}$ of the attraction is large enough so as to satisfy the above condition. In other words, the static edge DWs can exist if the correlation energy $-6g^{(ph)}$ overcomes the energy cost $E_k - E_q$ of a 1p-1h excitation. For $N = Z$ systems, one can regard the correlation of 1p-1h as that of four particles, because 1h corresponds to the three-particle state in the particle picture.

Let us consider the role of proton-neutron coherence in SSB. In the case that there is no proton-neutron interaction, the coupling $G^{(ph)}_{\chi,\chi'}$ is taken to be $G^{(ph)}_{\chi,\chi'} = g^{(ph)}\delta_{\tau\tau'}(1 - \delta_{\sigma\sigma'})$. Protons and neutrons are decoupled in the Hamiltonian, and the energy correction

$$E_{\rm corr} = 4\{(E_k - E_q)u^2 + 2g^{(ph)}u^2v^2\} \tag{33}$$

leads to the condition for SSB,

$$E_k - E_q < -2g^{(ph)}. \tag{34}$$

This condition is more difficult to satisfy than Eq. (32). This is the reason why the proton and neutron coherent edge DWs can be stable, while the incoherent neutron or proton edge DW is unfavored in the oblate 7α and 3α states. The reason for the smaller interaction term [i.e., a smaller correlation energy in Eq. (33) than in Eq. (29)] is that, in the particle picture, 1h corresponds to a one-particle state with no proton-neutron interaction, instead of the 1h state corresponding to a three-particle state with proton-neutron interactions.

We also consider the further unfavored proton edge DW in the neutron-rich system discussed in the previous section. Protons are deeply bound in the neutron-rich system, and therefore the energy cost $E_k - E_q$ for the 1p-1h excitation becomes large in general. As a result, the condition $E_k - E_q < -2g^{(ph)}$ becomes severe, and the proton edge DW is suppressed largely in neutron-rich nuclei.

VI. SUMMARY AND OUTLOOK

Pentagon and triangle shapes in ^{28}Si and ^{12}C were discussed in relation with DWs at the edge of oblate states. In AMD calculations, the $K^\pi = 5^-$ band in ^{28}Si and the $K^\pi = 3^-$ band in ^{12}C are described by pentagon and triangle shapes, respectively. These negative-parity bands can be interpreted as the parity partners of the $K^\pi = 0^+$ ground bands and they are constructed from the parity-asymmetric-intrinsic states. The pentagon and triangle shapes originate in the 7α- and 3α-cluster structures.

We performed analysis of ideal cluster model wave functions using BB α-cluster wave functions and also extended BB wave functions, and we investigated the development of the pentagon and triangle shapes. It was found that the proton-neutron coherence is essential in the development of the pentagon and triangle structures of the oblate states in $Z = N$ nuclei. Without the proton-neutron coherent density oscillation, the pentagon and triangle shapes are suppressed. Needless to say, this is consistent with the features of light $Z = N$ nuclei, in which cluster structures are favored because of α-cluster formation. In the oblate state of neutron-rich C, the triangle cluster structure is suppressed.

In the analysis of single-particle orbits of the AMD wave functions and BB α cluster wave functions, the pentagon and triangle shapes are regarded as static one-dimensional DWs at the edge of the oblate states. The edge DWs can be described by nonuniform orbits with parity mixing, which give density oscillation with wave numbers of five and three at the surface of the $0\hbar\omega$ oblate states.

The static edge DWs of the oblate $Z = N$ nuclei are understood by the spontaneous symmetric breaking of rotational invariance around the symmetric axis of the oblate states. In other words, the development of the 7α- and 3α-cluster

structures is interpreted as the instability of axial symmetry with respect to the pentagon and the triangle shapes. We introduced a simplified model and discussed SSB for the edge DWs. The development and the suppression of the pentagon and triangle structures are described by SSB inducing static edge DWs.

In the simplified model, the $0\hbar\omega$ oblate states are assumed to be the Hartree-Fock vacuua $|0\rangle_{\rm F}$. The model space for particle and hole states are truncated so that only $\phi_{(0,0,\pm3)}\mathcal{X}_{\tau\sigma}$ and $\phi_{(0,0,\pm2)}\mathcal{X}_{\tau\sigma}$ are active. Assuming a contact interaction, we adopted the DW term $H_{\rm DW}$ as the residual interaction. For the proton-neutron coherent edge DWs in $Z = N$ systems, SSB occurs when the condition $E_k - E_q < -6g^{(ph)}$ is satisfied. If there is no coupling between protons and neutrons, the condition for SSB is $E_k - E_q < -2g^{(ph)}$, which is a more severe condition than the proton-neutron coherent case. This means that the proton and neutron coherent edge DWs are favored, while an incoherent neutron or proton edge DW is unfavored.

Considering the condition $E_k - E_q < -2g^{(ph)}$ for an incoherent edge DW, we explained the reasons why the triangle cluster structure is suppressed in the oblate state of neutron-rich C. Since protons are deeply bound in neutron-rich nuclei, the level spacing of proton orbits becomes large. This increases the energy cost $E_k - E_q$ for a 1p-1h excitation, and hence the correlation energy $-2g^{(ph)}$ due to the triangle structure is not able to overcome the cost $E_k - E_q$.

The scenario for the suppression of the proton DW in neutron-rich systems could be extended also to infinite matter problems. Consider instability with respect to proton density oscillations in neutron-rich matter, symmetric nuclear matter, and pure proton matter with the same Fermi momentum of protons and ignoring the Coulomb force. Proton density waves should be most unfavored in neutron-rich matter among these three cases and might be favored with coherent neutron DWs in symmetric nuclear matter. It turns out that the possibility of α-cluster crystallization in neutron-rich matter may be suspicious. Alternatively, we can say that the α-cluster crystallization may be suppressed in neutron-rich matter because of the quenched effective mass of protons.

In the present simplified model, in which active orbits are limited to be a small number, DWs may be superior to BCS-type pairing in $Z = N$ systems. We adopted the ansatz of the residual interaction $H_2 = H_{\rm DW}$ and discuss the edge DWs in relation to SSB. This ansatz may be applicable only to the case when the level density is low enough, active orbits are restricted to almost one dimension, and the spin-orbit force can be ignored. Oblate ^{12}C may satisfy this condition and oblate ^{28}Si would probably do so. However, we should comment that, in normal nuclei, static surface DWs may yield to BCS pairing. The spin-orbit force may also weaken static DWs. Moreover, when the number of active orbits is large enough, BCS pairing overcomes DWs. Therefore, in heavy-mass nuclei, especially in spherical nuclei, BCS pairing can be predominant, as is well known. In fact, various phenomena resulting from BCS pairing have been observed in heavy-mass nuclei and are successfully described by BCS theory in the j-j coupling scheme.

ACKNOWLEDGMENTS

The computational calculations of this work were performed using the supercomputers at YITP and through the Supercomputer Projects of the High Energy Accelerator Research Organization (KEK). This work was supported by a Grant-in-Aid for Scientific Research from the Japan Society for the Promotion of Science (JSPS). It was also supported by a Grant-in-Aid for the Global COE Program "The Next Generation of Physics, Spun from Universality and Emergence" from the Ministry of Education, Culture, Sports, Science and Technology (MEXT) of Japan. Discussions during the YITP workshops and the YIPQS long-term workshops held at YITP were helpful for completing this work.

APPENDIX A: H.O. SINGLE-PARTICLE STATES

To see the relation between BB cluster wave functions and shell-model wave functions, it is convenient to expand a BB wave function with LS-coupling shell-model wave functions which are described in terms of single-particle orbits in the spherical H.O. potential. For instance, an α cluster located at the origin is expressed by four nucleons, $p\uparrow$, $p\downarrow$, $n\uparrow$, and $n\downarrow$, occupying the $0s$ orbit in the H.O. potential with frequencies $\omega_x = \omega_y = \omega_z = \omega \equiv \hbar/mb^2$. Here the parameter b is related to ν of the cluster wave functions as $\nu = 1/2b^2$. For oblate systems, it is convenient to use the expression of single-particle orbits with cylinder coordinates, $\rho = \sqrt{x^2 + y^2}$, z, ϕ, where z is the symmetry axis. Then, H.O. single-particle orbits are characterized by quantum numbers n_z, n_ρ, and m_l. Here n_z and n_ρ are the node numbers with respect to z and ρ coordinates and m_l is the eigenvalue for the z component of the orbital angular momentum. The total quantum number is $N = n_z + 2n_\rho + |m_l|$.

The explicit forms of the H.O. single-particle orbits $\phi_{(n_z,n_\rho,m_l)}$ for $(n_z, n_\rho, m_l) = (0, 0, \pm1)$, $(0, 0, \pm2)$, and $(0, 0, \pm3)$ are

$$\begin{aligned}
\phi_{(0,0,\pm1)}(\mathbf{r}) &= \frac{\mp1}{(\pi b^2)^{3/4}}\frac{\rho}{b}e^{\pm i\phi}e^{-r^2/2b^2},\\
\phi_{(0,0,\pm2)}(\mathbf{r}) &= \frac{1}{\sqrt{2}(\pi b^2)^{3/4}}\left(\frac{\rho}{b}\right)^2 e^{\pm 2i\phi}e^{-r^2/2b^2},\\
\phi_{(0,0,\pm3)}(\mathbf{r}) &= \frac{\mp1}{\sqrt{6}(\pi b^2)^{3/4}}\left(\frac{\rho}{b}\right)^3 e^{\pm 3i\phi}e^{-r^2/2b^2}.
\end{aligned} \tag{A1}$$

APPENDIX B: PARTICLE AND HOLE REPRESENTATION

In this appendix, we summarize the notations of the particle and hole representation. The creation and annihilation operators, $c_\alpha^\dagger$ and c_α, for a state $|\alpha\rangle$ are defined as

$$\begin{aligned}
c_\alpha^\dagger|-\rangle &= |\alpha\rangle,\\
c_\alpha|\alpha\rangle &= |-\rangle,\\
c_\alpha^\dagger|\alpha\rangle &= 0,\\
c_\alpha|-\rangle &= 0,
\end{aligned} \tag{B1}$$

where $|-\rangle$ is the no-particle state, and α denotes the index of all degrees of freedom of the single-particle state such as momentum, spin, and isospin. c_α and $c_\beta^\dagger$ satisfy $\{c_\alpha, c_\beta^\dagger\} = \delta_{\alpha,\beta}$, and other anticommutation relations are zero. To describe particle-hole excitations on the HF vacuum, we define the HF vacuum state as

$$|0\rangle_F \equiv \prod_{\alpha<F} c_\alpha^\dagger |-\rangle \tag{B2}$$

and the particle and hole operators as

$$\begin{aligned} a_\alpha^\dagger &= c_\alpha^\dagger && \text{for} \quad \alpha > F, \\ b_\alpha^\dagger &= S_{-\alpha} c_{-\alpha} && \text{for} \quad \alpha < F, \\ a_\alpha &= c_\alpha && \text{for} \quad \alpha > F, \\ b_\alpha &= S_{-\alpha} c_{-\alpha}^\dagger && \text{for} \quad \alpha < F. \end{aligned} \tag{B3}$$

Here $\alpha < F$ and $\alpha > F$ mean the states below and above the Fermi surface, respectively. The time reversal state of $|\alpha\rangle$ is defined as $S_{-\alpha}|-\alpha\rangle$.

For an infinite matter of spin-1/2 fermions, single-particle states can be characterized by momentum k and spin $s_z = \sigma$. In a usual convention, $|-\alpha\rangle = |-k, -\sigma\rangle$ for $|\alpha\rangle = |k, \sigma\rangle$ and

$$S_\alpha \equiv (-1)^{\frac{1}{2}-\sigma_\alpha}. \tag{B4}$$

For a spherically symmetric system, single-particle states can be characterized by the quantum numbers $|\alpha\rangle \equiv |nlsjm_j\rangle$ in the j-j coupling picture, and the corresponding $|-\alpha\rangle$ and the phase convention are

$$\begin{aligned} |-\alpha\rangle &= |nlsj - m_j\rangle, \\ S_\alpha &\equiv (-1)^{j-m_j}. \end{aligned} \tag{B5}$$

In an axial symmetric system in the l-s coupling scheme such as the present 7α and 3α models for ^{28}Si and ^{12}C, we use the notation $|\alpha\rangle = |n_z n_\rho m_l \sigma\rangle$ specified by the quantum numbers in cylinder coordinates and adopt the following conventions:

$$\begin{aligned} |-\alpha\rangle &= |n_z n_\rho - m_l - \sigma\rangle, \\ S_\alpha &\equiv (-1)^{\frac{1}{2}-\sigma-m_l}. \end{aligned} \tag{B6}$$

The operator $b_\alpha^\dagger$ creates a hole carrying the z component of angular momentum m_l and the spin $s_z = \sigma$.

We consider the Hamiltonian including the two-body interaction,

$$\begin{aligned} H &= \sum_{\alpha\beta} \langle\alpha|T|\beta\rangle c_\alpha^\dagger c_\beta + \frac{1}{2}\sum_{\alpha\beta\gamma\delta} \mathcal{V}_{\alpha,\beta,\gamma,\delta} c_\alpha^\dagger c_\beta^\dagger c_\gamma c_\delta, \\ \mathcal{V}_{\alpha,\beta,\gamma,\delta} &\equiv \frac{1}{2}\{\langle\alpha\beta|v|\gamma\delta\rangle - \langle\alpha\beta|v|\delta\gamma\rangle\}. \end{aligned} \tag{B7}$$

We rewrite the Hamiltonian in normal-ordered form with respect to new particle and hole operators assuming that the single-particle states, α, are solutions of Hartree-Fock single-particle equations, which diagonalize the Hamiltonian matrix

$$\langle\beta|T|\delta\rangle + \sum_{\alpha<F}[\langle\alpha\beta|v|\alpha\delta\rangle - \langle\alpha\beta|v|\delta\alpha\rangle] = E_\beta \delta_{\beta\delta}. \tag{B8}$$

Then the Hamiltonian takes the form

$$H = H_0 + H_1 + H_2, \tag{B9}$$

with

$$\begin{aligned} H_0 &= \sum_{\alpha<F}\langle\alpha|T|\alpha\rangle + \frac{1}{2}\sum_{\alpha<F}\sum_{\beta<F}[\langle\alpha\beta|v|\alpha\beta\rangle \\ &\quad -\langle\alpha\beta|v|\beta\alpha\rangle], \\ H_1 &= \sum_{\alpha>F} E_\alpha a_\alpha^\dagger a_\alpha - \sum_{\alpha<F} E_\alpha b_\alpha^\dagger b_\alpha, \\ H_2 &= \frac{1}{2}\sum_{\alpha\beta\gamma\delta} \mathcal{V}_{\alpha,\beta,\gamma,\delta} N(c_\alpha^\dagger c_\beta^\dagger c_\delta c_\gamma), \end{aligned} \tag{B10}$$

where $N(\ \ )$ is the normal-ordered product with respect to the particle and hole operators defined before. The residual interaction H_2 contains the particle-particle, hole-hole, and particle-hole scattering,

$$\begin{aligned} H_{pp} &= \frac{1}{2}\sum_{\alpha,\beta,\gamma,\delta>F} \mathcal{V}_{\alpha,\beta,\gamma,\delta} a_\alpha^\dagger a_\beta^\dagger a_\delta a_\gamma, \\ H_{hh} &= \frac{1}{2}\sum_{\alpha,\beta,\gamma,\delta<F} \mathcal{V}_{\alpha,\beta,\gamma,\delta} b_\alpha^\dagger b_\beta^\dagger b_\delta b_\gamma, \\ H_{ph} &= 2\sum_{\alpha,\gamma>F}\sum_{\beta,\delta<F} \mathcal{V}_{\alpha,-\delta,-\beta,\gamma} S_{-\beta} S_{-\delta} a_\alpha^\dagger b_\beta^\dagger b_\delta a_\gamma. \end{aligned} \tag{B11}$$

APPENDIX C: HAMILTONIAN OF THE SIMPLIFIED MODEL

We introduce a simplified model for the oblate state $\Phi_{7\alpha}^{(0\hbar\omega)}$. In this model, $\Phi_{7\alpha}^{(0\hbar\omega)}$ is assumed to be the HF vacuum $|0\rangle_F$, and possible particle-hole excitations are restricted within the HF single-particle states of $|\phi_{(0,0,\pm k)}\mathcal{X}_{\tau\sigma}\rangle$ and $|\phi_{(0,0,\pm q)}\mathcal{X}_{\tau\sigma}\rangle$. This means that the model space is truncated so that active orbits are only $|\phi_{(0,0,\pm k)}\mathcal{X}_{\tau\sigma}\rangle$ for particle states and $|\phi_{(0,0,\pm q)}\mathcal{X}_{\tau\sigma}\rangle$ for hole states with $k = 3$ and $q = 2$ (or $k = 2$ and $q = 1$ for the $\Phi_{3\alpha}^{(0\hbar\omega)}$). We use the labels $\alpha = \pm k, \tau\sigma$ and $\alpha = \pm q, \tau\sigma$ for these active single-particle states and also adopt the notation $\chi \equiv \tau\sigma$ and $-\chi \equiv \tau - \sigma$. In this paper, we define the particle and hole operators as

$$\begin{aligned} a_{\pm k,\chi}^\dagger &= c_{\pm k,\chi}^\dagger, \\ b_{\pm q,\chi}^\dagger &= c_{\mp q,-\chi}. \end{aligned} \tag{C1}$$

Here, for convenience, we adopt the definition of the hole operators without the phase convention instead of Eq. (B3).

In this model, we assume a contact two-body attraction $v(r) = g\delta(r)$ with $g < 0$ for the residual interaction in the H_2 term. The matrix element $V_{\alpha,\beta,\gamma,\delta}$ is not zero only when $k_\alpha + k_\beta = k_\gamma + k_\delta$ and $\chi_\alpha = \chi_\gamma \neq \chi_\beta = \chi_\delta$ (or $\chi_\alpha = \chi_\delta \neq \chi_\beta = \chi_\gamma$) are satisfied and calculated to be

$$\begin{aligned} G_{\chi\chi'}^{(pp)} &\equiv V_{k\chi,-k\chi',k\chi,-k\chi'} = g^{(pp)}(1-\delta_{\chi\chi'}), \\ g^{(pp)} &\equiv \frac{g}{2}\langle k,-k|\delta(r)|k,-k\rangle, \\ G_{\chi\chi'}^{(hh)} &\equiv V_{q\chi,-q\chi',q\chi,-q\chi'} = g^{(hh)}(1-\delta_{\chi\chi'}), \end{aligned}$$

$$
\begin{aligned}
g^{(hh)} &\equiv \frac{g}{2}\langle q,-q|\delta(r)|q,-q\rangle,\\
G^{(ph)}_{\chi\chi'} &\equiv V_{k\chi,-q\chi',k\chi,-q\chi'} = g^{(ph)}(1-\delta_{\chi\chi'}),\\
g^{(ph)} &\equiv \frac{g}{2}\langle k,-q|\delta(r)|k,-q\rangle.
\end{aligned}
\tag{C2}
$$

For the case of $k=3$ and $q=2$, one can get $g^{(pp)} = g^{(ph)} = 5g^{(hh)}/6 = 5g/(\pi^{3/2}b^3 2^6\sqrt{2})$. Thus, $g^{(pp)}$, $g^{(ph)}$, and $g^{(hh)}$ are almost equal to each other. Using the symmetry (or antisymmetry) of the matrix elements $V_{\alpha,\beta,\gamma,\delta}$ with respect to indexes, the Hamiltonian equation (B10) in the particle-hole representation can be rewritten in the explicit form

$$
\begin{aligned}
H &= H_0 + H_1 + H_2,\\
H_0 &= {}_{\rm F}\langle 0|H|0\rangle_{\rm F},\\
H_1 &= \sum_{\chi} E_{k,\chi} a^\dagger_{+k,\chi} a_{+k,\chi} + \sum_{\chi} E_{k,\chi} a^\dagger_{-k,\chi} a_{-k,\chi}\\
&\quad - \sum_{\chi} E_{q,\chi} b^\dagger_{+q,\chi} b_{+q,\chi} - \sum_{\chi} E_{k,\chi} b^\dagger_{-q,\chi} b_{-q,\chi},\\
H_2 &= H^{ph} + H^{pp} + H^{hh},
\end{aligned}
\tag{C3}
$$

with

$$
\begin{aligned}
H^{ph} &= 2\sum_{\chi,\chi'} G^{(ph)}_{\chi,\chi'}[a^\dagger_{+k,\chi} b^\dagger_{+q,-\chi} b_{+q,-\chi'} a_{+k,\chi'}\\
&\quad + a^\dagger_{-k,\chi} b^\dagger_{-q,-\chi} b_{-q,-\chi'} a_{-k,\chi'}\\
&\quad + a^\dagger_{+k,\chi} b^\dagger_{-q,-\chi} b_{-q,-\chi'} a_{+k,\chi'}\\
&\quad + a^\dagger_{-k,\chi} b^\dagger_{+q,-\chi} b_{+q,-\chi'} a_{-k,\chi'}]\\
&\quad - 2\sum_{\chi,\chi'} G^{(ph)}_{\chi,\chi'}[a^\dagger_{+k,\chi} b^\dagger_{+q,-\chi'} b_{+q,-\chi'} a_{+k,\chi}\\
&\quad + a^\dagger_{-k,\chi} b^\dagger_{-q,-\chi'} b_{-q,-\chi'} a_{-k,\chi}\\
&\quad + a^\dagger_{+k,\chi} b^\dagger_{-q,-\chi'} b_{-q,-\chi'} a_{+k,\chi}\\
&\quad + a^\dagger_{-k,\chi} b^\dagger_{+q,-\chi'} b_{+q,-\chi'} a_{-k,\chi}],
\end{aligned}
\tag{C4}
$$

$$
\begin{aligned}
H^{pp} &= \sum_{\chi,\chi'} G^{(pp)}_{\chi,\chi'}[a^\dagger_{+k,\chi} a^\dagger_{+k,\chi'} a_{+k,\chi'} a_{+k,\chi}\\
&\quad + a^\dagger_{-k,\chi} a^\dagger_{-k,\chi'} a_{-k,\chi'} a_{-k,\chi}]\\
&\quad + 2\sum_{\chi,\chi'} G^{(pp)}_{\chi,\chi'}[a^\dagger_{+k,\chi} a^\dagger_{-k,\chi'} a_{-k,\chi'} a_{+k,\chi}\\
&\quad + a^\dagger_{+k,\chi} a^\dagger_{-k,\chi'} a_{+k,\chi'} a_{-k,\chi}],
\end{aligned}
\tag{C5}
$$

$$
\begin{aligned}
H^{hh} &= \sum_{\chi,\chi'} G^{(hh)}_{\chi,\chi'}[b^\dagger_{+q,\chi} b^\dagger_{+q,\chi'} b_{+q,\chi'} b_{+q,\chi}\\
&\quad + b^\dagger_{-q,\chi} b^\dagger_{-q,\chi'} b_{-q,\chi'} b_{-q,\chi}]\\
&\quad + 2\sum_{\chi,\chi'} G^{(hh)}_{\chi,\chi'}[b^\dagger_{+q,\chi} b^\dagger_{-q,\chi'} b_{-q,\chi'} b_{+q,\chi}\\
&\quad + b^\dagger_{+q,\chi} b^\dagger_{-q,\chi'} b_{+q,\chi'} b_{-q,\chi}],
\end{aligned}
\tag{C6}
$$

where we omit $0\to 4$ and $1\to 3$ and their inverse processes. In the particle-hole interaction term H^{ph}, the DW term

$$
\begin{aligned}
H_{\rm DW} &\equiv 2\sum_{\chi,\chi'} G^{(ph)}_{\chi,\chi'}[a^\dagger_{+k,\chi} b^\dagger_{+q,-\chi} b_{+q,-\chi'} a_{+k,\chi'}\\
&\quad + a^\dagger_{-k,\chi} b^\dagger_{-q,-\chi} b_{-q,-\chi'} a_{-k,\chi'}]
\end{aligned}
\tag{C7}
$$

may induce the edge DWs having the wave number $\pm(k+q)$, which gives the nonzero expectation value $\langle a^\dagger_{\pm k,\chi} b^\dagger_{\pm q,-\chi}\rangle$. The terms of $a^\dagger_{\pm k,\chi} b^\dagger_{\mp q,-\chi} b_{\mp q,-\chi'} a_{\pm k,\chi'}$ in H^{ph} may induce the exciton mode having the wave number ± 1. They contain the spurious mode of translational motion and are of no interest in finite systems. Other terms in H^{ph} have the opposite sign and they do not give coherent effects to the correlation energy.

In H^{pp} and H^{hh}, the interactions which may induce the BCS pairing are the following terms:

$$
\begin{aligned}
H^{pp}_{\rm BCS} &= 2\sum_{\chi,\chi'} G^{(pp)}_{\chi,\chi'}[a^\dagger_{+k,\chi} a^\dagger_{-k,\chi'} a_{-k,\chi'} a_{+k,\chi}\\
&\quad + a^\dagger_{+k,\chi} a^\dagger_{-k,\chi'} a_{+k,\chi'} a_{-k,\chi}],
\end{aligned}
\tag{C8}
$$

$$
\begin{aligned}
H^{hh}_{\rm BCS} &= 2\sum_{\chi,\chi'} G^{(hh)}_{\chi,\chi'}[b^\dagger_{+q,\chi} b^\dagger_{-q,\chi'} b_{-q,\chi'} b_{+q,\chi}\\
&\quad + b^\dagger_{+q,\chi} b^\dagger_{-q,\chi'} b_{+q,\chi'} b_{-q,\chi}].
\end{aligned}
\tag{C9}
$$

In the case of $Z=N$ nuclei, only two types of BCS pairing, for instance, $a^\dagger_{+k,p\uparrow} a^\dagger_{-k,p\downarrow}$ and $a^\dagger_{+k,n\uparrow} a^\dagger_{-k,n\downarrow}$, are usually considered among four species of nucleons, $\chi = p\uparrow, p\downarrow, n\uparrow, n\downarrow$. This is different from the DWs induced by $H_{\rm DW}$ where four types of particle-hope combination, $\langle a^\dagger_{\pm k,\chi} b^\dagger_{\pm q,-\chi}\rangle$, can be nonzero simultaneously and they can give coherent effects to the correlation energy. Since the coupling constants $G^{(ph)}$, $G^{(pp)}$, and $G^{(hh)}$ are of the same order, the DW may be superior to the BCS-type pairing in $Z=N$ systems in the present simplified model with a limited number of active orbits. We consider $H_{\rm DW}$ to be the dominant term, and we adopt the ansatz of $H_2 = H_{\rm DW}$ and discuss the edge DWs in the Hamiltonian $H = H_0 + H_1 + H_{\rm DW}$ in relation to the SSB.

APPENDIX D: ALTERNATIVE METHOD TO SOLVE THE DW HAMILTONIAN

In this appendix, we solve Eq. (24) in the approximation, omitting the quantum fluctuation of the product of the particle and hole operators. This is a kind of mean-field approach in field theory. We show that the same results as those in Sec. V are obtained in this approximation.

Let us consider $H = H_0 + H_1 + H_{\rm DW}$ in Eq. (24). By decomposing $H_{\rm DW}$ into mean fields and their fluctuations, we can rewrite the second and third terms, $H_1 + H_{\rm DW}$, as

$$
\begin{aligned}
H_1 + H_{\rm DW} &= H_{\rm mf} + H_{\rm quasi} + H_{\rm fluc},\\
H_{\rm mf} &\equiv -2\sum_{\chi,\chi'} G^{(ph)}_{\chi,\chi'}[\langle a^\dagger_{+k,\chi} b^\dagger_{+q,-\chi}\rangle\langle b_{+q,-\chi'} a_{+k,\chi'}\rangle\\
&\quad + \langle a^\dagger_{-k,\chi} b^\dagger_{-q,-\chi}\rangle\langle b_{-q,-\chi'} a_{-k,\chi'}\rangle],
\end{aligned}
$$

$$
\begin{aligned}
H_{\rm quasi} \equiv\ & H_1 + 2\sum_{\chi,\chi'} G^{(ph)}_{\chi,\chi'}[a^\dagger_{+k,\chi} b^\dagger_{+q,-\chi} \langle b_{+q,-\chi'} a_{+k,\chi'}\rangle \\
& + \langle a^\dagger_{+k,\chi} b^\dagger_{+q,-\chi}\rangle b_{+q,-\chi'} a_{+k,\chi'} \\
& + a^\dagger_{-k,\chi} b^\dagger_{-q,-\chi} \langle b_{-q,-\chi'} a_{-k,\chi'}\rangle \\
& + \langle a^\dagger_{-k,\chi} b^\dagger_{-q,-\chi}\rangle b_{-q,-\chi'} a_{-k,\chi'}], \\
H_{\rm fluc} \equiv\ & 2\sum_{\chi,\chi'} G^{(ph)}_{\chi,\chi'}[(a^\dagger_{+k,\chi} b^\dagger_{+q,-\chi} - \langle a^\dagger_{+k,\chi} b^\dagger_{+q,-\chi}\rangle) \\
& \times (b_{+q,-\chi'} a_{+k,\chi'} - \langle b_{+q,-\chi'} a_{+k,\chi'}\rangle) \\
& + (a^\dagger_{-k,\chi} b^\dagger_{-q,-\chi} - \langle a^\dagger_{-k,\chi} b^\dagger_{-q,-\chi}\rangle) \\
& \times (b_{-q,-\chi'} a_{-k,\chi'} - \langle b_{-q,-\chi'} a_{-k,\chi'}\rangle)], \qquad \text{(D1)}
\end{aligned}
$$

where $H_{\rm mf}$, $H_{\rm quasi}$, and $H_{\rm int}$ are the mean-field energy term, the sum of H_1 and the interaction term between particles and the mean field, and the fluctuation term of the mean field, respectively. In the mean-field approximation, $H_{\rm fluc}$ is assumed to be negligible, so we drop $H_{\rm fluc}$. We also assume that the ground state does not break time-reversal symmetry, so that the mean fields satisfy

$$
\langle b_{+q,-\chi} a_{+k,\chi}\rangle = -\langle a^\dagger_{-k,-\chi} b^\dagger_{-q,\chi}\rangle. \qquad \text{(D2)}
$$

The Hamiltonian of the quasiparticle $H_{\rm quasi}$ can be written as

$$
\begin{aligned}
H_{\rm quasi} =\ & \sum_\chi (a^\dagger_{+k,\chi}\ b_{+q,\chi}\ a^\dagger_{-k,\chi}\ b_{-q,\chi}) \\
& \times \begin{pmatrix} E_{k,\tau} & \Delta_\chi & 0 & 0 \\ \Delta^*_\chi & E_{q,\tau} & 0 & 0 \\ 0 & 0 & E_{k,\tau} & -\Delta^*_{-\chi} \\ 0 & 0 & -\Delta_{-\chi} & E_{q,\tau} \end{pmatrix} \begin{pmatrix} a_{+k,\chi} \\ b^\dagger_{+q,\chi} \\ a_{-k,\chi} \\ b^\dagger_{-q,\chi} \end{pmatrix} \\
& - 2\sum_\chi E_{q,\tau}, \qquad \text{(D3)}
\end{aligned}
$$

where the last term in Eq. (D3) comes from the anticommutation relation $b^\dagger_{\pm q,\chi} b_{\pm q,\chi} = -b_{\pm q,\chi} b^\dagger_{\pm q,\chi} + 1$. The gap is defined by

$$
\Delta_\chi \equiv 2\sum_{\chi'} G_{\chi,\chi'} \langle b_{q,-\chi'} a_{k,\chi'}\rangle. \qquad \text{(D4)}
$$

Since $H_{\rm quasi}$ depends on Δ_χ, the right-hand side in Eq. (D4) also depends on Δ_χ through the expectation value; thus, Eq. (D4) can be regarded as a self-consistency equation. The Hamiltonian of the quasiparticle has a quadratic form, so it can be diagonalized by the following unitary transformation or Bogoliubov transformation:

$$
\begin{aligned}
\begin{pmatrix} \tilde a_{+k,\chi} \\ \tilde b^\dagger_{+q,\chi} \end{pmatrix} &= \begin{pmatrix} v_\chi & -u_\chi \\ u^*_\chi & v^*_\chi \end{pmatrix} \begin{pmatrix} a_{+k,\chi} \\ b^\dagger_{+k,\chi} \end{pmatrix}, \\
\begin{pmatrix} \tilde a_{-k,\chi} \\ \tilde b^\dagger_{-q,\chi} \end{pmatrix} &= \begin{pmatrix} v^*_\chi & u^*_\chi \\ -u_\chi & v_\chi \end{pmatrix} \begin{pmatrix} a_{-k,\chi} \\ b^\dagger_{-k,\chi} \end{pmatrix},
\end{aligned} \qquad \text{(D5)}
$$

with

$$
\frac{u_\chi}{v_\chi} = \frac{-2\Delta_\chi}{E_{k,\tau} - E_{q,\tau} + \sqrt{(E_{k,\tau} - E_{q,\tau})^2 + 4|\Delta_\chi|^2}}, \qquad \text{(D6)}
$$

which satisfies $|v_\chi|^2 + |u_\chi|^2 = 1$. The eigenvalues of $H_{\rm quasi}$ corresponding to the energies of the quasiparticles are

$$
\begin{aligned}
\tilde E_{k,\chi}(\Delta_\chi) &= \frac{1}{2}\Big(E_{k,\tau} + E_{q,\tau} + \sqrt{(E_{k,\tau} - E_{q,\tau})^2 + 4|\Delta_\chi|^2}\Big), \\
\tilde E_{q,\chi}(\Delta_\chi) &= \frac{1}{2}\Big(E_{k,\tau} + E_{q,\tau} - \sqrt{(E_{k,\tau} - E_{q,\tau})^2 + 4|\Delta_\chi|^2}\Big).
\end{aligned} \qquad \text{(D7)}
$$

The new vacuum is defined as the state vanished by the annihilation operators $\tilde a_{\pm k,\chi}$ and $\tilde b_{\pm q,\chi}$:

$$
\tilde a_{\pm k,\chi}|\Psi\rangle = \tilde b_{\pm q,\chi}|\Psi\rangle = 0. \qquad \text{(D8)}
$$

The solution of Eq. (D8) is given by

$$
\begin{aligned}
|\Psi(\Delta_\chi)\rangle =\ & \prod_\chi (v_\chi + u_\chi a^\dagger_{+k,\chi} b^\dagger_{+k,\chi}) \\
& \times \prod_\chi (v^*_\chi - u^*_\chi a^\dagger_{-k,\chi} b^\dagger_{-k,\chi})|0\rangle_{\rm F}. \qquad \text{(D9)}
\end{aligned}
$$

This has the same form as Eq. (25); however, they are different, because the vacuum in Eq. (D9) is a function of Δ_χ, while that in Eq. (25) is a function of u_τ (and v_τ), which is a variational parameter. Their vacua coincide at the solutions of the self-consistent equation and the variational equation.

The expectation value of $H_{\rm quasi}$ becomes

$$
E_{\rm quasi}(\Delta_\chi) = \langle H_{\rm quasi}\rangle = 2\sum_\chi (\tilde E_{q,\chi}(\Delta_\chi) - E_{q,\chi}), \qquad \text{(D10)}
$$

where $E_{\rm quasi}(\Delta_\chi) \leqslant 0$ and the equality is only satisfied when $|\Delta_\chi| = 0$. The mean-field term can be rewritten by Δ_χ as

$$
H_{\rm mf} = -\sum_{\chi,\chi'} \frac{1 - 3\delta_{\chi,\chi'}}{3g^{(ph)}} \Delta^*_\chi \Delta_{\chi'}, \qquad \text{(D11)}
$$

where we used the explicit form of the interaction $G^{(ph)}_{\chi\chi'} = g^{(ph)}(1 - \delta_{\chi,\chi'})$. Using Eqs. (D10) and (D11), we obtain the correlation energy as

$$
\begin{aligned}
2E_{\rm corr}(\Delta_\chi) &= E_{\rm quasi} + H_{\rm mf} \\
&= 2\sum_\chi \Bigg(\tilde E_{q,\chi}(\Delta_\chi) - E_{q,\chi} \\
&\quad - \sum_{\chi'} \frac{1 - 3\delta_{\chi,\chi'}}{6g^{(ph)}} \Delta^*_\chi \Delta_{\chi'}\Bigg). \qquad \text{(D12)}
\end{aligned}
$$

In the mean-field approximation, Δ_χ is obtained by the stationary condition

$$
\begin{aligned}
\frac{\partial}{\partial \Delta^*_\chi} E_{\rm corr}(\Delta_\chi) &= \frac{-\Delta_\chi}{\sqrt{(E_{k,\tau} - E_{q,\tau})^2 + 4|\Delta_\chi|^2}} \\
&\quad + \frac{\Delta_\chi}{2g^{(ph)}} - \frac{\sum_{\chi'} \Delta_{\chi'}}{6g^{(ph)}} \\
&= 0. \qquad \text{(D13)}
\end{aligned}
$$

Notice that Eq. (D13) is the equivalent to the consistency condition Eq. (D4), which can be checked by inserting $\langle b_{q,-\chi} a_{k,\chi}\rangle = u_\chi v_\chi$.

For $Z = N$ systems, when $E_{k,\tau}$ and $E_{q,\tau}$ are independent of the isospin, Δ_χ is independent of χ. The solution is

$$\Delta_\chi = 3g\sqrt{1 - \frac{(E_k - E_q)^2}{(6g)^2}}. \tag{D14}$$

Inserting Eq. (D14) into Eqs. (D6) and (D12), one finds that v_τ and u_τ coincide with Eq. (31) and also that $E_{\rm corr}$ coincides with Eq. (29).

[1] D. M. Brink, in *Proceedings of the International School of Physics Enrico Fermi 36*, edited by C. Bloch (Academic Press, New York, London, 1966), p. 247.
[2] T. Yukawa and S. Yoshida, Phys. Lett. B **33**, 334 (1970).
[3] H. Horiuchi and K. Ikeda, in *Cluster Models and Other Topics, International Review of Nuclear Physics* (World Scientific, Singapore, 1987), Vol. 4, p. 1.
[4] F. Ajzenberg-Selove, Nucl. Phys. A **506**, 1 (1990).
[5] E. Uegaki, S. Okabe, Y. Abe, and H. Tanaka, Prog. Theor. Phys. **54**, 1262 (1977).
[6] F. Glatz *et al.*, Z. Phys. A **303**, 239 (1981).
[7] W. Bauhoff, Z. Phys. A **305**, 187 (1982).
[8] W. Bauhoff *et al.*, Phys. Rev. C **26**, 1725 (1982).
[9] J. A. Maruhn, M. Kimura, S. Schramm, P. G. Reinhard, H. Horiuchi, and A. Tohsaki, Phys. Rev. C **74**, 044311 (2006).
[10] Y. Kanada-En'yo, Phys. Rev. C **71**, 014303 (2005).
[11] Y. Kanada-En'yo, M. Kimura, and H. Horiuchi, Nucl. Phys. A **734**, 341 (2004).
[12] A. W. Overhauser, Phys. Rev. Lett. **4**, 415 (1960).
[13] M. de Llano, Nucl. Phys. A **317**, 183 (1979).
[14] H. Ui and Y. Kawazore, Z. Phys. A **301**, 125 (1981).
[15] D. M. Brink and J. J. Castro, Nucl. Phys. A **216**, 109 (1973).
[16] A. Tohsaki-Suzuki, Prog. Theor. Phys. **81**, 370 (1989).
[17] H. Takemoto, M. Fukushima, S. Chiba, H. Horiuchi, Y. Akaishi, and A. Tohsaki, Phys. Rev. C **69**, 035802 (2004).
[18] Y. Kanada-Enyo and H. Horiuchi, Prog. Theor. Phys. **93**, 115 (1995); Y. Kanada-Enyo, H. Horiuchi, and A. Ono, Phys. Rev. C **52**, 628 (1995); Y. Kanada-Enyo and H. Horiuchi, *ibid.* **52**, 647 (1995).
[19] Y. Kanada-En'yo and H. Horiuchi, Prog. Theor. Phys. Suppl. **142**, 205 (2001).
[20] Y. Kanada-En'yo, M. Kimura and H. Horiuchi, C. R. Phys. **4**, 497 (2003).
[21] T. Ando, K. Ikeda, and A. Tohsaki, Prog. Theor. Phys. **64**, 1608 (1980).
[22] N. Yamaguchi, T. Kasahara, S. Nagata, and Y. Akaishi, Prog. Theor. Phys. **62**, 1018 (1979); R. Tamagaki, *ibid.* **39**, 91 (1968).
[23] A. Doté, H. Horiuchi and Y. Kanada-En'yo, Phys. Rev. C **56**, 1844 (1997).
[24] J. Bardeen, L. N. Cooper, and J. R. Schrieffer, Phys. Rev. **108**, 1175 (1957).
[25] R. Tamagaki and T. Takatsuka, Prog. Theor. Phys. **56**, 1340 (1976).
[26] T. Takatsuka, K. Tamiya, T. Tatsumi, and R. Tamagaki, Prog. Theor. Phys. **59**, 1933 (1978).
[27] A. B. Migdal, Rev. Mod. Phys. **50**, 107 (1978).
[28] F. Dautry and E. M. Nyman, Nucl. Phys. A **319**, 323 (1979).
[29] D. V. Deryagin, D. Y. Grigoriev, and V. A. Rubakov, Int. J. Mod. Phys. A **7**, 659 (1992).
[30] E. Shuster and D. T. Son, Nucl. Phys. B **573**, 434 (2000).
[31] B. Y. Park, M. Rho, A. Wirzba, and I. Zahed, Phys. Rev. D **62**, 034015 (2000).
[32] M. G. Alford, J. A. Bowers, and K. Rajagopal, Phys. Rev. D **63**, 074016 (2001).
[33] E. Nakano and T. Tatsumi, Phys. Rev. D **71**, 114006 (2005).
[34] I. Giannakis and H. C. Ren, Phys. Lett. B **611**, 137 (2005).
[35] K. Fukushima, Phys. Rev. D **73**, 094016 (2006).
[36] D. Nickel, Phys. Rev. Lett. **103**, 072301 (2009); Phys. Rev. D **80**, 074025 (2009).
[37] T. Kojo, Y. Hidaka, L. McLerran, and R. D. Pisarski, Nucl. Phys. A **843**, 37 (2010).
[38] S. Carignano, D. Nickel, and M. Buballa, Phys. Rev. D **82**, 054009 (2010).
[39] K. Fukushima and T. Hatsuda, Rep. Prog. Phys. **74**, 014001 (2011).
[40] G. Gruner, Rev. Mod. Phys. **60**, 1129 (1988).
[41] G. Gruner, Rev. Mod. Phys. **66**, 1 (1994).